Limits and constraints on mechanisms of cell-cycle regulation imposed by cell size-homeostasis measurements

Lisa Willis[1,*], Henrik Jönsson[2,3], Kerwyn Casey Huang[1,4,5,*]

[1]Department of Bioengineering, Stanford University, Stanford, CA 94305, USA

[2]Sainsbury Laboratory, University of Cambridge, Cambridge, CB2 1LR, UK

[3]Department of Applied Mathematics and Theoretical Physics, University of Cambridge, Cambridge, CB3 0DZ, UK

[4]Department of Microbiology and Immunology, Stanford University, Stanford, CA 94305, USA

[5]Chan Zuckerberg Biohub, San Francisco, CA 94158, USA

*Correspondence: lisawillis@stanford.edu, kchuang@stanford.edu

Lead contact: kchuang@stanford.edu

Summary

High-throughput imaging has led to an explosion of observations regarding cell-size homeostasis across the kingdoms of life. Among bacteria, "adder" behavior in which a constant size appears to be added during each cell cycle is ubiquitous, while various eukaryotes show other size-homeostasis behaviors. Since interactions between cell-cycle progression and growth ultimately determine size-homeostasis behaviors, we developed a general model of cell proliferation to: 1) discover how the requirement of cell-size homeostasis limits mechanisms of cell-cycle control; 2) predict how features of cell-cycle control translate into size-homeostasis measurements. Our analyses revealed plausible cell-cycle control scenarios that nevertheless fail to regulate cell size, conditions that generate apparent adder behavior without underlying adder mechanisms, cell-cycle features that play unintuitive roles in causing deviations from adder, and distinguishing predictions for extended size-homeostasis statistics according to the underlying control mechanism. The model thus provides holistic insight into the mechanistic implications of cell-size homeostasis measurements.

Keywords: *Cell-size homeostasis, cell growth, cell-cycle checkpoints, CDK1-cyclin activity, Whi5, FtsZ, DnaA, inhibitor dilutor, mechanistic models, phenomenological models*

Introduction

One of the most fundamental questions in biology is how cells regulate cell-cycle progression, which is intimately tied to myriad processes such as cell-size determination (Schmoller et al., 2015), drug sensitivity (Shi et al., 2017), and transcription (Padovan-Merhard et al., 2015). In all organisms, cell-cycle control must be coupled to growth to ensure cell-size homeostasis, the maintenance of a fixed average size in steady conditions. Measurable size-homeostasis behaviors are determined by interactions between cell-cycle control and growth. Single-cell lineage tracking and cell-cycle reporters have led to a rapid proliferation in size homeostasis measurements across bacteria, yeast, mammalian cells, and plant cells. Among bacteria (Campos et al., 2014; Taheri-Araghi et al., 2015; Wallden et al., 2016; Willis and Huang, 2017) and an archaeon (Eun et al., 2018), a common theme has emerged: cells appear to regulate their size via an "adder" behavior whereby a fixed volume is added between birth and division. Among eukaryotes, budding yeast and mammalian cells can deviate from adder behavior over the G1 and S/G2 cell-cycle stages while maintaining apparent adder or near-adder behavior between birth and division (Cadart et al., 2018; Chandler-Brown et al., 2017; Di Talia et al., 2007; Schmoller et al., 2015), with the smallest mammalian cells switching to approximately "sizer" behavior with no correlation between birth and division sizes (Varsano et al., 2017). Similarly, small fission yeast exhibit sizer behavior at division while large fission yeast exhibit near-adder behaviour

(Facchetti et al., 2019; Fantes, 1977; Pan et al., 2014). By contrast, stem cells of *Arabidopsis thaliana* exhibit intermediate adder-sizer behavior (Willis et al., 2016).

Despite the recent explosion of size-homeostasis measurements, there is no clarity as to the implications of these similarities and differences for mechanisms of cell-cycle control and its coupling to growth. Furthermore, despite the centrality of these concepts, how the necessity for size homeostasis limits mechanisms of cell-cycle control is not understood. We sought to develop a theoretical framework to address two major questions: how does the requirement for cell-size homeostasis limit cell-cycle regulator dynamics and mechanisms of cell-cycle checkpoint progression, and to what extent are size-homeostasis measurements informative about underpinning mechanisms of cell-cycle regulation? Importantly, it is unresolved whether the widely observed "adder" behavior implies a common mechanism across diverse organisms.

Seminal studies have revealed how cell-cycle progression is coupled to growth in several model organisms. In budding yeast, the G1/S inhibitor Whi5 is produced throughout S/G2/M and then diluted out by growth during G1 to trigger G1/S upon reaching a threshold minimum concentration (Schmoller et al., 2015). Mathematical models showed that for budding yeast-like proliferation dynamics, this "inhibitor-dilutor" G1/S regulation imparts adder behavior between birth and division (Chandler-

Brown et al., 2017; Heldt et al., 2018; Soifer et al., 2016). Whi5 has functional homologs in mammals (Rb) and plants (RBR1), suggesting that an inhibitor-dilutor mechanism may regulate G1/S. In the bacterium *Escherichia coli*, the division protein FtsZ is a "master regulator" of division, with newly synthesized FtsZ accumulating at midcell proportionally with cell growth to trigger division at a total intracellular threshold level (Sekar et al., 2018; Si et al., 2019), a mechanism that recapitulates the observed adder behavior. Similarly, active DnaA, which accumulates at the origins of replication, effects adder behavior both between consecutive G1/Ss and between consecutive divisions if it is produced proportionally with growth and triggers replication initiation (G1/S) at a threshold level per origin when it is inactivated while a fixed time or added-size increment elapses between G1/S and division (Amir, 2014; Barber et al., 2017; Ho and Amir, 2015; Logsdon et al., 2017). DnaA followed by a fixed time interval and FtsZ mediated division may operate simultaneously, with the slower process triggering cell division (Micali et al., 2018a; Micali et al., 2018b; Si et al., 2019). DnaA and FtsZ are broadly conserved among bacteria but details of their dynamics and other proliferation factors are likely to vary; the extent to which size homeostasis limits their dynamics, and how they can account for the apparent universality of adder behavior across bacteria are unclear. Master regulators also control cell cycle-checkpoint progression in eukaryotes: the broadly conserved CDK1-cyclin (Harashima et al., 2013) accumulates during growth to trigger G1/S then G2/M at successive threshold activity levels in

engineered fission yeast (Coudreuse and Nurse, 2010). The CDK1-cyclin regulatory network is complex, but data indicate that it may result in a simple scaling relating active CDK1-cyclin accumulation to cell size (Keifenheim et al., 2017; Patterson et al., 2019).

Here, we develop a general model of cell proliferation and thus predict the size-homeostasis behaviors produced by a wide range of cell-cycle control mechanisms. Instances of the model focus on cells with two phases partitioned by the major eukaryotic cell-cycle checkpoints: G1/S and G2/M (assuming that G2/M and division are coincident), and on two rate-limiting mechanisms of irreversible checkpoint progression: master regulators like CDK1-cyclin or FtsZ/DnaA that accumulate to threshold activity levels, and Whi5-like inhibitor dilutors. Previous models have focused on particular organisms with specific cell-cycle and growth regimes, and thus do not provide a comprehensive framework connecting proliferation dynamics to size-homeostasis measurements, or do not consider the mechanism coupling growth and cell-cycle progression and therefore lack predictive power for how genetic perturbations will affect size-homeostasis behavior. We systematically identify apparently plausible cell-cycle control scenarios that nevertheless fail to regulate cell size and are thus impossible. We describe how growth, noise origins, cell cycle checkpoint criteria, and cell-cycle regulator dynamics differentially impact size

114 homeostasis measurements, and how additional size homeostasis measurements may
115 be useful to discriminate among different underlying mechanisms that cause robust
116 deviation from adder, as observed in *A. thaliana*. Taken together, this framework and
117 the insights it provides should be broadly useful for interpreting and motivating cell-
118 size homeostasis measurements across all organisms.

Results

A general model of cell proliferation with two cell-cycle checkpoints

Our models consider two types of checkpoint regulators motivated by present understanding of the eukaryotic cell cycle (Fig. 1A): 1) a master regulator (e.g., CDK1-cyclin) that accumulates from zero and triggers G1/S or G2/M progression upon reaching a total intracellular threshold level (absolute number of molecules), when it is immediately degraded; 2) an inhibitor dilutor (e.g. Whi5) that accumulates during one phase and is diluted out in the subsequent phase, triggering progression upon reaching a threshold minimum concentration with no subsequent degradation. Master regulators can accumulate through one phase, as is common for cyclins in eukaryotes, or two phases, as for CDK1-cyclin in an engineered model of fission yeast (Coudreuse and Nurse, 2010; Hochegger et al., 2008) and FtsZ/DnaA in slow-growing bacteria without multiple replication forks. Regulator production rates (dC/dt) can be cell-size dependent and may differ between phases according to

$$\frac{dC}{dt} = \kappa_{\text{phase}}\, S^{\lambda_{c,\text{phase}}}$$

where C is the number of proteins, S is cell size, and $\lambda_{c,\text{phase}}$, κ_{phase} are parameters (Fig. 1A). Production rates change with cell size continually through the phase if $\lambda_{c,\text{phase}} \neq 0$. The majority of proteins are thought to be maintained at constant concentrations during steady-state growth and thus likely are produced at a fixed rate proportional to cell size

in exponentially growing cells ($\lambda_{c,\mathrm{phase}} = 1$) (Newman et al., 2006; Padovan-Merhard et al., 2015; Schmoller and Skotheim, 2015), while Whi5 is produced independently of size through S/G2/M in budding yeast ($\lambda_{c,\mathrm{S/G2/M}} = 0$) (Schmoller et al., 2015), and in fission yeast the activity of CDK1-cyclin may increase with a stronger size-dependence ($\lambda_{c,\mathrm{phase}} > 1$) that results from multiple regulators with cell size-dependent levels (Keifenheim et al., 2017). The ratio of regulator production rates ($r_{\mathrm{S/G2/M}} = \kappa_{\mathrm{S/G2/M}}/\kappa_{\mathrm{G1}}$) represents two extreme scenarios: either production is gene-copy number limited, meaning that the production rate doubles in S/G2/M upon gene duplication regardless of ploidy ($r_{\mathrm{S/G2/M}} = 2$), or production is unaffected by gene-copy number ($r_{\mathrm{S/G2/M}} = 1$) because another factor such as ribosome abundance is limiting (Heldt et al., 2018; Schmoller and Skotheim, 2015; Schmoller et al., 2015) (Fig. 1A). Proteins are assumed to be stable, consistent with measurements of key regulators, aside from targeted degradation (Hochegger et al., 2008; Schmoller et al., 2015). If a regulator persists through cell divisions, we assume it is inherited in proportion to daughter cell sizes without noise.

In our model, cells divide into sisters with size-ratio 1:($\sigma - 1$). Thus, binary fission and asymmetric division are accounted for by $\sigma = 2$ and $\sigma \neq 2$, respectively (Fig. 1B), and at steady state cells increase their average birth size by an average factor σ over the cell cycle. The growth rate (dS/dt) can be cell-size dependent according to

159 $$\frac{dS}{dt} = \gamma S^{\lambda_g}.$$

160 While many organisms grow exponentially ($\lambda_g = 1$) (Di Talia et al., 2007; Osella et al.,
161 2014; Soifer et al., 2016; Taheri-Araghi et al., 2015; Wang et al., 2010; Willis et al., 2016),
162 there is some evidence of linear growth in certain regimes ($\lambda_g = 0$) (Lin and Amir, 2018).
163 γ sets the average timescale for growth; $\ln \sigma / \gamma$ is the average cell cycle duration for
164 exponential growth (Fig. 1C).

165

166 We consider master regulators or inhibitor dilutors of G1/S or G2/M in combination
167 with various phenomenological controls over S/G2/M or G1, respectively, including
168 sizer, adder, or timer control, meaning that over the phase in question cells reach a
169 critical size, add a fixed size increment, or a fixed time period elapses. Specifically, cell
170 size at the end of the phase ($S_{\mathrm{e,phase}}$) is determined by cell size at the beginning of the
171 phase ($S_{\mathrm{i,phase}}$) according to

172 $$S_{\mathrm{e,phase}} = f_{\mathrm{phase}}\, S_{\mathrm{i,phase}} + (\sigma_{\mathrm{phase}} - f_{\mathrm{phase}})\, \mu_{\mathrm{i,phase}}$$

173 where f_{phase} is the mode of control ($f_{\mathrm{phase}} = 0$, 1, or σ_{phase} for sizer, adder, or timer
174 control and exponential growth, respectively), $\sigma_{\mathrm{phase}} > 1$ is the average fold-size
175 increase, and $\mu_{\mathrm{i,phase}}$ is the average initial size at steady state (Fig. 1D). We call phases
176 that follow this size-determination rule independently regulated. The average fraction
177 of the cell cycle spent in G1 at steady state (τ, which equals the G1 duration $\times\ \gamma / \ln \sigma$ for
178 exponential growth) and the mode of division (σ) determine $\sigma_{\mathrm{G1}} \approx \sigma^{\tau}$ and $\sigma_{\mathrm{S/G2/M}} \approx$

179 $\sigma^{1-\tau}$ because $\sigma = \sigma_{\mathrm{G1}}\,\sigma_{\mathrm{S/G2/M}}$ (the approximations are exact for exponential growth,
180 Methods). Average sizes at birth ($\mu_{\mathrm{i,G1}}$) and G1/S ($\mu_{\mathrm{i,S/G2/M}}$) are determined by a
181 combination of parameters governing the average regulator dynamics ($\lambda_{c,\mathrm{phase}}$, κ_{phase})
182 and threshold levels or concentrations, G1 duration (τ), growth type (λ_g, γ), and
183 division behavior (σ) (Table S1, SI). Cell-size fluctuations emerge from noise in
184 regulator dynamics, noise in the critical levels or concentrations that trigger cell-cycle
185 progression, and noise in sizer/adder/timer mechanisms. The impact of noise on size-
186 homeostasis behavior is encapsulated by two parameters ($\eta_{\mathrm{G1/S}}$ and $\eta_{\mathrm{G2/M}}$; Methods and
187 SI) according to

188 $$\eta_{\mathrm{checkpoint}} = \frac{\text{Noise in the transition's checkpoint mechanism}}{\text{Coefficient of variation (CV) in G1/S size}}$$

189 (Fig. 1E). For example, assuming typical values of the CV of G1/S size of ~13% (Cadart
190 et al., 2018; Taheri-Araghi et al., 2015; Willis et al., 2016), a typical error of ~7% in a G1/S
191 threshold concentration checkpoint gives $\eta_{\mathrm{G1/S}}$~0.5, and a typical error of ~20% in a
192 S/G2/M timer checkpoint gives $\eta_{\mathrm{G2/M}}$~0.5 assuming exponential growth, binary fission,
193 and $\tau = 0.5$ (Methods and SI). Fig. 1F summarizes the parameters affecting size-
194 homeostasis. In later sections, motivated by findings in *A. thaliana*, mammalian cells,
195 and bacteria (Cadart et al., 2018; Ginzberg et al., 2018; Nordholt et al., 2019; Willis et al.,
196 2016), growth and production rates are allowed to depend on cell birth size, and the
197 threshold mechanisms for cell-cycle checkpoint progression are generalized.

198

199 Together, this model represents a broad framework for interrogating the requirements
200 and molecular bases for cell-size homeostasis measurements.
201
202 **G1/S inhibitor dilutors combined with S/G2/M sizer or timer regulation fail to**
203 **achieve size homeostasis in plausible cell proliferation scenarios**
204 It is well known that master regulators of G2/M produced at a constant, size-
205 independent rate throughout both phases fail to achieve size homeostasis in
206 exponentially growing cells: a fixed time elapses between divisions, and cells multiply
207 their birth size by a constant factor on average prior to division, so that cells born large
208 get larger while small cells get smaller (Willis and Huang, 2017). We applied our model
209 to identify other cell proliferation scenarios that fail to achieve G1/S or G2/M size
210 homeostasis. We temporarily set noise sources to zero to determine whether
211 homeostasis is lost independently of noise. To maintain homeostasis at steady G1/S and
212 G2/M mean sizes, G1/S and G2/M size fluctuations must regress to their respective
213 means, which requires that the absolute value of the slope between sizes at consecutive
214 G1/S and G2/M transitions is <1 (Fig. S1). For example, the G2/M size-homeostasis
215 requirement fails if a fixed time period T elapses between birth and division while cells
216 grow exponentially:

217 $$\text{G2/M size at generation } n+1 = (\text{birth size at generation } n+1)e^{\gamma T}$$

218 $$= \frac{\text{G2/M size at generation } n}{\sigma} e^{\gamma T} = \text{G2/M size at generation } n$$

because at steady state $e^{\gamma T} = \sigma$; hence the slope between consecutive G2/M sizes is 1 and fluctuations do not decay to the mean. The loss of size homeostasis occurs despite the fixed cell cycle duration. Below, we readily identify more complex conditions that fail to regulate size by analytically deriving these slopes in terms of model parameters (Methods, SI).

In exponentially growing budding yeast, Whi5 executes inhibitor-dilutor control of G1/S, with Whi5 produced at a constant rate through S/G2/M, and an approximately fixed interval elapses between G1/S and G2/M (Schmoller et al., 2015). If S/G2/M is under timer control and growth is exponential, our model predicts that an inhibitor produced in proportion to cell size or growth ($\lambda_{c,\mathrm{S/G2/M}} = \lambda_g = 1$; Fig. 1A,C) or with a stronger size-dependency ($\lambda_{c,\mathrm{S/G2/M}} \geq 1$) fails to regulate both G1/S and G2/M sizes (Fig. 2Ai,ii, Table S2). Single-cell trajectories with realistic noise levels illustrate this loss of size control as $\lambda_{c,\mathrm{S/G2/M}}$ varies from 0 (constant production rate) to 1 (proportional to size) (Fig. 2Bi-iv) while the G1 and S/G2/M durations and thus the ordering of G1/S and G2/M are maintained so cells contain the correct number of genome copies. By contrast, if S/G2/M were under adder control, size homeostasis is achieved for $\lambda_{c,\mathrm{S/G2/M}} = 0$ and 1 (Fig. 2Aiii,iv).

Regardless of the type of growth and inhibitor production, the inhibitor threshold concentration for G1/S, and the division pattern, we also found that G1/S inhibitor dilutors are incompatible with G2/M sizer mechanisms and long G1 durations ($\tau \geq 0.5$): for $\tau \approx 0.5$, fluctuations below the average G1/S size are overcompensated for in the subsequent generation (Fig. 2Av,vi), consistent with analytical predictions of a slope between consecutive G1/S sizes ≤-1 (Fig. S1, Table S2), so G1/S size homeostasis is lost and transitions frequently alternate between the beginning and end of the cell cycle (arrows in Fig. 2Bv,vi). Analogous results apply for inhibitor dilutors that trigger G2/M rather than G1/S with timer/adder/sizer control over G1 (SI). The model's generality and analytical tractability enabled these results, which demonstrate how cell proliferation scenarios that are *a priori* biologically plausible necessarily fail to achieve size homeostasis and thus can be ruled out.

Master regulators can lose cell-size control when production is gene copy-number limited or strongly size-dependent, or when a threshold concentration triggers phase progression

CDK1-cyclin and DnaA/FtsZ cell-cycle regulation are thought to be widely conserved in eukaryotes and bacteria, respectively, but details of the regulators' dynamics and other proliferation factors have yet to be quantified in nearly all species. Motivated by CDK1-cyclin and DnaA/FtsZ, we focused on G2/M and G1/S master regulators produced

through both phases ("two-phase" master regulators) and applied our model to identify limits on proliferation dynamics imposed by size homeostasis.

For exponentially growing cells, when regulator production is gene copy-number limited ($r_{\mathrm{S/G2/M}} = 2$; Fig. 1A), G2/M two-phase master regulators produced at a size-independent rate ($\lambda_{c,\mathrm{G1/S}} = \lambda_{c,\mathrm{S/G2/M}} = 0$) fail to execute size homeostasis for G1 timer control, because then a fixed time elapses over the cell cycle which is incompatible with exponential growth regardless of other parameters (Fig. 3Ai). However, we found that size homeostasis is restored for G1 sizer or adder control (Fig. 3Aii,iii, Table S2) largely regardless of the average G1 duration (τ). By contrast, G1/S two-phase master regulators that are gene copy-number limited are incompatible with G2/M sizer regulation: this combination fails to implement G1/S size homeostasis for binary fission or asymmetric division ($\sigma \leq 2$) (Fig. 3B, Table S2). This finding depends on the increased rate of regulator production during S/G2/M due to gene-copy number doubling and, conditional upon no growth rate (γ) increase during S/G2/M, holds regardless of the average G1 duration and the size-dependencies of production and growth (λ_g and $\lambda_{c,\mathrm{phase}}$, assuming $\lambda_{c,\mathrm{G1}} = \lambda_{c,\mathrm{S/G2/M}}$) (SI). Here, the loss of G1/S size homeostasis while G2/M size homeostasis is enforced implies that the proper ordering of G1/S followed by G2/M is also lost (Fig. S2). G1/S two-phase master regulators produced at a strongly size-dependent rate throughout the cell cycle without being

gene copy-number limited ($\lambda_c = \lambda_{c,\mathrm{G1}} = \lambda_{c,\mathrm{S/G2/M}} \geq 2 + \lambda_g$, $r_{\mathrm{S/G2/M}} = 1$) fail to execute G1/S size homeostasis for S/G2/M timer regulation combined with binary fission or asymmetric division ($\sigma \geq 2$) and long S/G2/M durations ($1 - \tau \geq 0.6$) (Fig. 3Ci, iv). For $\lambda_c = 2 + \lambda_g$ but not $\lambda_c = 3 + \lambda_g$, size homeostasis is restored by S/G2/M adder or sizer regulation (Fig. 3C, Table S2). Thus, under exponential growth, G1/S two-phase master regulators such as DnaA robustly achieve size homeostasis only when $0 < \lambda_c < 3$.

While size homeostasis is achieved by two-phase master regulators produced from an initial level of zero in proportion to growth ($\lambda_{c,\mathrm{G1}} = \lambda_{c,\mathrm{S/G2/M}} = \lambda_g$, $r_{\mathrm{S/G2/M}} = 1$) to trigger phase progression at a threshold level (Amir, 2014), we found that if instead progression is triggered at a critical concentration (or a local threshold density in an intracellular region that scales proportionally with cell size), size homeostasis is generally lost (Fig. 3D, SI). This mechanism fails because a threshold concentration means that cell size at the checkpoint is proportional to the regulator's level, which is proportional to the added size since production is proportional to growth. Thus, cell size at the checkpoint is proportional to the added size, and ultimately cells multiply their birth size by a constant factor on average prior to division, so there is no negative feedback on size fluctuations. However, if the size-dependence of regulator production exceeds that of growth ($\lambda_{c,\mathrm{phase}} > \lambda_g$), size homeostasis can be restored (SI). Thus, to

297 maintain size homeostasis in bacteria, the division-initiating FtsZ midcell bands must
298 not increase in width proportionally as the cell grows.
299
300 In all cases above, analytical predictions were confirmed by simulations of single-cell
301 trajectories with realistic size fluctuations (Fig. 2B, 3D, S2). A recurring theme is that
302 switching to adder regulation of S/G2/M or G1 restored size homeostasis when sizer or
303 timer regulation failed (white regions in Fig. 2A, 3A,B,C). Thus, these scenarios
304 illustrate robustness of adder regulation, regardless of its molecular origin.
305
306 **Connecting cell-cycle regulation mechanisms to linear regression slopes between**
307 **birth and division sizes**
308 When taking noise into account, we can predict how regulatory factors affect size-
309 homeostasis behaviors at steady state by deriving linear regression slopes between birth
310 and division sizes and among other size variables (Methods). We present particular
311 scenarios motivated by experiment (see SI for the general case).
312
313 At least in *E. coli*, DnaA appears to operate as a two-phase master regulator between
314 consecutive G1/Ss (Si et al., 2019), while in slow growth conditions S/G2/M is
315 independently regulated by a timer or adder mechanism or a mechanism whereby both
316 a minimum time period elapses and a minimum size increment is added between

317 divisions (Logsdon et al., 2017; Micali et al., 2018b). Then, the linear regression slope of
318 birth vs. division size is

319 $$(1) \qquad \left(\sigma_{\mathrm{G1}}^{\lambda_g-\lambda_c} - r_{\mathrm{S/G2/M}}\sigma_{\mathrm{S/G2/M}}^{\lambda_c-\lambda_g}\right) f_{\mathrm{S/G2/M}} + r_{\mathrm{S/G2/M}} \frac{\left(\frac{f_{\mathrm{S/G2/M}}}{\sigma_{\mathrm{S/G2/M}}}\right)^2}{\left(\frac{f_{\mathrm{S/G2/M}}}{\sigma_{\mathrm{S/G2/M}}}\right)^2 + \eta_{\mathrm{G2/M}}^2}$$

320 where $\lambda_c = \lambda_{c,\mathrm{G1}} = \lambda_{c,\mathrm{S/G2/M}}$ represents the regulator's size-dependent production,
321 which we assume to be constant throughout the cell cycle, and recalling $\sigma_{\mathrm{G1}} \approx \sigma^{\tau} \approx$
322 $\sigma/\sigma_{\mathrm{S/G2/M}}$ (Fig. 1F, Methods). From Eq. 1, and in agreement with other studies (Amir,
323 2014; Ho and Amir, 2015), a production rate that is proportional to growth ($\lambda_c = \lambda_g$,
324 $r_{\mathrm{S/G2/M}} = 1$) combined with low G2/M checkpoint noise vs. other sources of cell size
325 noise ($\eta_{\mathrm{G2/M}} \ll 1$) and supra-sizer control of G2/M ($f_{\mathrm{S/G2/M}} > 0$) gives a slope ~1, which
326 means that apparent adder behavior (slope=1) is predicted regardless of further
327 constraints on the S/G2/M control mechanism ($f_{\mathrm{S/G2/M}}$) (Fig. 4A). $\eta_{\mathrm{G2/M}}$ is small when cell
328 size fluctuations are primarily from noise sources other than the G2/M checkpoint, for
329 example, from fluctuations in regulator production (Fig. 1E). Under exponential
330 noiseless growth, a typical error $e_{\mathrm{G2/M}}$ in a S/G2/M timer checkpoint (CV of S/G2/M
331 duration, SI) dictates that $\eta_{\mathrm{G2/M}} = e_{\mathrm{G2/M}} \ln \sigma_{\mathrm{S/G2/M}} / (\mathrm{CV\ of\ G1/S\ size})$, so for $e_{\mathrm{G2/M}} = 10\%$,
332 $\sigma_{\mathrm{S/G2/M}} \approx \sigma^{1-\tau} \approx 1.4$, and a CV of G1/S size = 13%, then $\eta_{\mathrm{G2/M}}^2 \approx 0.06$ has a nominal
333 effect on the slope in Eq. 1 (Fig. 4A).
334

335 In engineered fission yeast, CDK1-cyclin is produced through G1 and S/G2/M to trigger
336 G2/M at a threshold prior to degradation (Coudreuse and Nurse, 2010), while in *E. coli*
337 FtsZ accumulates at midcell up to a threshold level to trigger G2/M or division (Si et al.,
338 2019); in both cases, G2/M is likely controlled by a two-phase master regulator. The
339 corresponding linear regression slope of birth vs. division size is

340 $$(2) \qquad \sigma^{\lambda_g-\lambda_c}\, r_{\mathrm{S/G2/M}}^{-1} + \sigma_{\mathrm{S/G2/M}}^{\lambda_g-\lambda_c}(1 - r_{\mathrm{S/G2/M}}^{-1})\, f_{\mathrm{G1}},$$

341 producing adder behavior when production and growth rates are proportional
342 throughout the cell cycle ($\lambda_c = \lambda_g$; $r_{\mathrm{S/G2/M}} = 1$) regardless of other parameters. For
343 strongly size-dependent production ($\lambda_c > \lambda_g$), from Eq. 2, G2/M master regulators
344 asymptote to slopes of ~0 and thus to apparent sizer behaviors regardless of other
345 parameters (Fig. 4B). By contrast, from Eq. 1, for $\lambda_c \approx \lambda_g + 2$, G1/S two-phase master
346 regulators tend to produce strongly negative slopes corresponding to oscillatory size
347 behaviors where the average is overshot then undershot (Fig. 4C).

348

349 Eq. 1 indicates that high G2/M checkpoint noise ($\eta_{\mathrm{G2/M}}^2$~1) invariably reduces the slope
350 of G1/S two-phase master regulators, an effect that can be understood qualitatively.
351 High $\eta_{\mathrm{G2/M}}$ and a non-noisy coupling between growth and regulator dynamics entail
352 that cells born small contain less master regulator and therefore must produce more
353 regulator over G1 and correspondingly grow more to achieve the threshold level for
354 G1/S (Fig. 4D). For timer/adder/intermediate sizer-adder regulation of S/G2/M, any

355 compensatory growth over G1 is inherited as a positive fluctuation in G2/M-added size.
356 Thus, the slope between birth and division is reduced by noisy G2/M checkpoint
357 control, and this effect can be masked by other processes that contribute to G1/S size
358 fluctuations without coupling G1/S size to birth size, such as noisy production of the
359 G1/S regulator. By contrast, the slope in Eq. 2 is unaffected by noise levels (SI): noise
360 impacts the size-homeostasis behaviors between birth and division of G1/S regulators
361 because the production and persistence of the regulator through G2, mitosis, and
362 division correlates birth-size fluctuations with fluctuations in birth-regulator levels;
363 G2/M regulators are degraded or used up prior to birth, so there is no mechanism to
364 generate such a correlation.
365
366 These findings showcase the interplay of factors contributing to size-homeostasis
367 statistics and opposing predictions for G1/S vs. G2/M two-phase master regulators
368 concerning the effects of noise and size-dependent production.
369
370 **Noise levels dictate whether inhibitor dilutors achieve adder-like, sizer-like, or**
371 **supra-adder behaviors**
372 In budding yeast, various studies have identified adder-like behavior between birth and
373 division (Chandler-Brown et al., 2017; Di Talia et al., 2007; Soifer et al., 2016). However,
374 deletion of *CLN3*, which leads to prolonged G1 and increased average size (Cross, 1988),

375 or an additional copy of *WHI5* caused behavior closer to sizer for cells that were born
376 small (Chandler-Brown et al., 2017). Experiment and theory have shown that in the
377 absence of noise, the observed combination of constant production of the inhibitor
378 dilutor *WHI5* controlling G1/S, exponential cell growth, and timer control of S/G2/M can
379 result in apparent adder behavior (Chandler-Brown et al., 2017; Di Talia et al., 2007;
380 Heldt et al., 2018; Schmoller et al., 2015; Soifer et al., 2016), despite the lack of a
381 molecular adder underpinning the phenomenological behavior between birth and
382 division. Moreover, noise was suggested to have the potential to disrupt adder behavior
383 (Barber et al., 2017).
384
385 We applied our model to determine how noise and gene copy-number effects impact
386 size-homeostasis behaviors of budding yeast-like G1/S inhibitor dilutors. The linear
387 regression slope of G1/S size vs. overall added size until the next G1/S (ignoring the
388 intervening division) most easily discerns the size-homeostasis behavior between
389 consecutive G1/Ss: a slope of 0 indicates adder behavior. For exponential growth,
390 S/G2/M timer control, and constant inhibitor production through S/G2/M as in budding
391 yeast, the linear regression slope of G1/S size vs. overall added size until the next G1/S
392 is
393 $$-\eta_{\mathrm{G1/S}}^2, \qquad (3)$$
394 and the slope of birth vs. division size is

$$1 + \left(\frac{\sigma - 1}{\ln \sigma_{\mathrm{S/G2/M}}} - 1 \right) \eta_{\mathrm{G2/M}}^2 - \eta_{\mathrm{G1/S}}^2 \quad (4)$$

(Methods). From Eqs. 3 and 4, noise contributions affect size-homeostasis behaviors (Fig. 4E-G) while the inhibitor's production rate ($\kappa_{\mathrm{S/G2/M}}$) and threshold concentration for G1/S, which are feasibly altered by *WHI5* and *CLN3* copy numbers, have no impact. Apparent adder behaviors, corresponding to slopes of ~0 and ~1 in Eqs. 3 and 4, respectively, are observed only for relatively stringent G1/S checkpoint control: for a typical error in the inhibitor's G1/S threshold concentration of $e_{\mathrm{G1/S}} = 10\%$, $\eta_{\mathrm{G1/S}} = e_{\mathrm{G1/S}}/\mathrm{CV(G1/S\ size)} \approx 0.8$ (assuming $\mathrm{CV(G1/S\ size)} \approx 13\%$), so the slopes in Eqs. 3 and 4 are perturbed by $-0.8^2 = -0.64$ producing sub-adder behaviors (Fig. 4E,G); whereas for a comparable typical error in the S/G2/M timer checkpoint of $e_{\mathrm{G2/M}} = 10\%$, then $\eta_{\mathrm{G2/M}} = e_{\mathrm{G2/M}} \ln \sigma_{\mathrm{S/G2/M}} / \mathrm{CV(G1/S\ size)} = 0.25$ (assuming $\sigma = 2$ and $\sigma_{\mathrm{S/G2/M}} = \sigma^{1-\tau} = 2^{0.5} = 1.4$) and the slope in Eq. 4 is perturbed considerably less (by only +0.12, Fig. 4F) and near-adder behavior results. Among inhibitor dilutors, similar to G1/S two-phase master regulators (Eq. 1), adder behaviors require that size fluctuations are primarily from noise sources other than cell-cycle checkpoint mechanisms, such as fluctuations in inhibitor production and dilution.

The size-homeostasis behaviors in Eqs. 3 and 4 can be understood qualitatively. The key feature that results in apparent adder behavior between G1/Ss is the constant amount of

inhibitor produced over S/G2/M: the critical concentration at G1/S means that every inhibitor molecule corresponds to a small unit size s_0, so if n inhibitor molecules are produced over S/G2/M, the cell adds a size $n \times s_0$ to achieve the threshold concentration at the next G1/S (Fig. 4H) (Schmoller et al., 2015). Noise in either the inhibitor dynamics or the S/G2/M timer phase alters the number of inhibitor molecules produced during S/G2/M, and therefore causes the added size between consecutive G1/Ss to fluctuate, but this fluctuation is independent of the initial G1/S size. By contrast, fluctuations in the threshold concentration (the G1/S checkpoint) entail the opposite scenario; a high inhibitor threshold concentration corresponds to small cells at G1/S, so small cells must grow more than the average to dilute out the surplus inhibitor, leading to sub-adder behavior between G1/Ss. If G1/S size fluctuations arise entirely from G1/S checkpoint noise, then the relatively small noise in inhibitor production and S/G2/M interval means that daughter cells inherit a constant amount of inhibitor at birth, and the threshold concentration necessary for G1/S translates into a threshold cell size, resulting in apparent sizer regulation. These arguments apply to any inhibitor production rate and S/G2/M regulatory mode that together produce a constant amount of inhibitor during S/G2/M regardless of growth pattern and G1 duration, under the assumption of no inhibitor degradation following G1/S. Rapid inhibitor degradation following G1/S would produce sizer behavior between G1/Ss, since regardless of noise levels, the G1 regulator level would be uncoupled from the preceding G1/S size.

These findings indicate that G1/S inhibitor dilutors can exhibit adder, supra-adder, or sizer behavior depending on which processes make the primary contributions to cell-size fluctuations (Schmoller et al., 2015). Stringent control of the inhibitor's threshold concentration for G1/S is necessary for apparent adder behavior, and noise in this control may lead to sizer-like behaviors.

Deviations in regulator localization patterns cause supra-adder behaviors

Cell-cycle regulators can accumulate in a particular region of the cell, triggering checkpoint progression at a local threshold density. For example, in fission yeast the cell cycle regulator cdr2 accumulates at midcell to trigger division at a local threshold density (Facchetti et al., 2019; Pan et al., 2014). In this case, the threshold density mechanism effects a total intracellular threshold level criterion, because fission yeast grow as rods and the cdr2 localization region at midcell does not scale with size. Division in rod-shaped *E. coli* is regulated in an analogous way by FtsZ (Shi et al., 2017; Si et al., 2019). By contrast, the midcell diameters of coccoid bacteria and plant stem cells are not constant but increase with cell size (Willis et al., 2016), and in general cellular geometries and growth patterns vary among organisms.

453 To address the implications of heterogeneous localization, we derived the size-
454 homeostasis behaviors of G2/M two-phase master regulators that accumulate to a
455 threshold density within a cellular region that increases with cell size as $\sim S^{\lambda_T}$. The
456 region grows in proportion to size if $\lambda_T = 1$ (as do most nuclei), and (depending on
457 geometry) with surface area or midcell perimeter if $\lambda_T \approx 2/3$ or $1/3$. Then, assuming
458 $\lambda_c = \lambda_{c,\mathrm{G1}} = \lambda_{c,\mathrm{S/G2/M}}$ and $r_{\mathrm{S/G2/M}} = 1$ (Fig. 1F), the linear regression slope of birth vs.
459 division size is

460 $$\frac{\sigma^{\lambda_g-\lambda_c}}{1-\lambda_T\frac{\sigma^{\lambda_g-\lambda_c-1}-1}{\lambda_g-\lambda_c-1}} = \frac{1}{1-\lambda_T(1-\sigma^{-1})} \text{ for } \lambda_g = \lambda_c \quad (5)$$

461 (SI). From Eq. 5, because $\frac{\sigma^{\lambda_g-\lambda_c-1}-1}{\lambda_g-\lambda_c-1} > 0$, localization to a region that increases with size
462 ($\lambda_T > 0$) invariably increases the slope (Fig. 5A), predicting supra-adder behavior when
463 growth and regulator production are proportional ($\lambda_g = \lambda_c$) and intermediate sizer-
464 adder behavior when production is strongly size-dependent ($\lambda_c \gg 1$). Adder behavior is
465 achieved when a threshold concentration rather than level of regulator triggers G2/M
466 ($\lambda_T = 1$ vs. $\lambda_T = 0$ in Eq. 5) under the requirements that $\lambda_g < \lambda_c$ and $\lambda_g - \lambda_c =$
467 $\frac{1-\sigma^{-1}}{1-\sigma^{-(\lambda_g-\lambda_c)}}$ (≈ -0.7 for $\sigma = 2$) (Fig. 5B). We have been unable to identify plausible
468 mechanisms producing this relation, suggesting that threshold concentration
469 mechanisms are unlikely to underlie adder behavior.
470

Cell cycle inhibitors can also localize to subcellular regions, such as the localization of Whi5 to the nucleus for part of G1 in budding yeast (Di Talia et al., 2007). If an inhibitor dilutor localizes to a region that increases with cell size as $\sim S^{\lambda_T}$ and triggers G1/S upon reaching a threshold density within that region, the linear regression slope of birth vs. division size is

$$\sigma^{1-\lambda_T}\left(1+\left(\frac{\sigma^{\lambda_T}-1}{\lambda_T \ln \sigma_{\mathrm{S/G2/M}}}-1\right)\eta^2_{\mathrm{G2/M}}-\eta^2_{\mathrm{G1/S}}\right). \quad (6)$$

From Eq. 6, for stringent checkpoint control or noisy inhibitor dynamics ($\eta^2_{\mathrm{G1/S}}$ and $\eta^2_{\mathrm{G2/M}} \ll 1$), localization to any region that does not scale proportionally with size ($\lambda_T < 1$) increases the slope (Fig. 5C), again predicting supra-adder behavior (SI).

In summary, deviations in regulator localization patterns from the default scenarios (localization to a region that is proportional to size in inhibitor dilutors or independent of size in master regulators) increases the linear regression slope between birth and division sizes, tending to generate supra-adder behavior.

Apparent adder regulation between birth and division can be achieved with non-adder regulation over G1 and S/G2/M via independently regulated G1 or S/G2/M phases

Mammalian cells and budding yeast behave as apparent adders or near-adders between birth and division. However, the linear regression slopes between birth and G1/S sizes

491 (l_{G1}), and G1/S and G2/M or division sizes ($l_{S/G2/M}$), are significantly different from 1
492 (Cadart et al., 2018; Chandler-Brown et al., 2017; Schmoller et al., 2015), indicating
493 deviations from adder behavior over G1 and S/G2/M individually. In some strains, the
494 G1 size-homeostasis behavior is sub-adder, compensating for a supra-adder timer mode
495 of S/G2/M regulation to achieve an overall adder between birth and division (Cadart et
496 al., 2018).
497
498 To consider how cell proliferation mechanisms can give rise to G1 compensatory
499 behaviors, it was important to establish the consequences of independent regulation of
500 a phase (Fig. 1D). Eukaryotic cyclin-like regulators that are produced through only one
501 phase and degraded outside of this phase are likely to produce independently regulated
502 phases, because only size fluctuations at the beginning of the phase impact the
503 regulator's dynamics and thus size fluctuations at the end of the phase (Fig. 6A). For
504 independently regulated phases with control mode f_{phase}, the linear regression slope
505 between cell sizes at the beginning and end of the phase is $l_{phase} = f_{phase}$ (Methods). If
506 S/G2/M is independently regulated, the steady state linear regression slope of birth vs.
507 division size is
508 $$l_{G1}\, l_{S/G2/M} \qquad (7)$$
509 (SI). From Eq. 7, any mechanism that achieves apparent adder behavior between birth
510 and division must exhibit a G1 behavior that compensates for the S/G2/M regulation,

that is, $l_{\mathrm{G1}} = 1/l_{\mathrm{S/G2/M}}$, which causes a negative correlation between birth size and G1 duration (Fig. 6B, SI). Failure to satisfy Eq. 7, signifying deviation from G1 compensatory behavior, implies that S/G2/M is not independently regulated, likely because progression through S/G2/M is limited by molecular species that persist through multiple cell-cycle phases. Otherwise, if the independently regulated S/G2/M phase is noisy, the contribution of G2/M checkpoint noise to cell size fluctuations may alter the apparent size-homeostasis behavior between birth and G1/S (l_{G1}), because $\eta_{\mathrm{G2/M}}$ can affect linear regression slopes between birth and division (e.g. $\eta_{\mathrm{G2/M}} > f_{\mathrm{phase}}/\sigma_{\mathrm{phase}}$ in Eqs. 1 and 4) without affecting the mode of independently regulated S/G2/M control ($f_{\mathrm{S/G2/M}} = l_{\mathrm{S/G2/M}}$). By contrast, a stringently regulated independent phase ($\eta_{\mathrm{checkpoint}} \ll f_{\mathrm{phase}}/\sigma_{\mathrm{phase}}$) displays the same size-homeostasis behaviors between consecutive G2/Ms and consecutive G1/Ss at steady state (Fig. 6C, SI), regardless of other modeling assumptions. Then, Eq. 7 holds regardless of whether G1 or S/G2/M is the independently regulated phase, and any scenario that produces adder behavior over the cell cycle, between either birth and division or G1/Ss, produces the apparent G1 vs. S/G2/M compensatory behavior.

Size homeostasis measurements in the *A. thaliana* apical stem cell niche, an expanse of tissue at the plant apex that gives rise to all above-ground organs, established a linear

regression slope of birth vs. division size ≈ 0.5 (Willis et al., 2016) (Fig. 7A). No mechanistic model has previously been proposed to explain this intermediate behavior between sizer and adder. CDK1-cyclin species are highly conserved as major G1/S and G2/M regulators throughout eukaryotes, including *A. thaliana* (Scofield et al., 2014). Whi5 has no structural *A. thaliana* homolog, but the *A. thaliana* human retinoblastoma (RBR1) homolog plays a functional role similar to Whi5 (Harashima and Sugimoto, 2016; Turner et al., 2012), raising the possibility that *A. thaliana* G1/S is regulated by an inhibitor dilutor.

Since our model can generate homeostasis behaviors that vary continuously depending on factors such as regulator dynamics and noise levels, we applied Eqs. 1-7 to identify control mechanisms that could account for intermediate sizer-adder behavior. Here, we highlight five mechanisms taking into account that *A. thaliana* stem cells increase their average size by 1.5-fold over G1 ($\sigma_{\mathrm{G1}} = 1.5$) (Dewitte et al., 2003) and by 2-fold over the cell cycle ($\sigma = 2$), implying a 1.3-fold increase over S/G2/M ($\sigma_{\mathrm{S/G2/M}} = \frac{\sigma}{\sigma_{\mathrm{G1}}} = 1.3$), and grow exponentially throughout the cell cycle ($\lambda_g = 1$) at a per unit size rate that correlates negatively with birth size (Willis et al., 2016). To account for the negative correlation, we model growth rate dependence on birth size fluctuations as $\gamma\left(1 + \alpha_g \Delta S_{\mathrm{i,G1}}\right)$ and regulator production rate dependence on initial size fluctuations as $\kappa_{\mathrm{phase}}\left(1 + \alpha_{c,\mathrm{phase}} \Delta S_{\mathrm{i,phase}}\right)$, where $\Delta S_{\mathrm{i,phase}} = \frac{S_{\mathrm{i}}}{\mu_{\mathrm{i,phase}}} - 1$ is the scaled deviation from the

551 average size at the beginning of the phase ($\mu_{\mathrm{i,phase}}$) (SI). In *A. thaliana* stem cells, $\alpha_g \approx$
552 -0.5 (Willis et al., 2016) while $\alpha_{c,\mathrm{phase}}$ is unknown. This negative correlation is not
553 unique to plants; it has recently been observed in mammalian and bacterial cell lines
554 (Cadart et al., 2018; Nordholt et al., 2019). The hypothesized mechanisms are described
555 below, with distinguishing predictions for other measurable statistics: the linear
556 regression slopes between birth and G1/S sizes (l_{G1}), between G1/S and G2/M sizes
557 ($l_{\mathrm{S/G2/M}}$), and the relative CVs in G2/M size vs. G1/S size ($\rho_{\mathrm{G2/M\ vs.G1/S}}$) (Fig. 7B).
558
559 (1) A G2/M two-phase master regulator produced in proportion to cell size with no
560 gene-copy number or birth-size dependence ($\lambda_{c,\mathrm{phase}} = 1, r_{\mathrm{S/G2/M}} = 1, \alpha_{c,\mathrm{phase}} = 0$)
561 generates a linear regression slope of birth vs. division size of
562 $$1 + \alpha_g\,(\sigma - 1) \qquad (8)$$
563 regardless of the mode of G1/S regulation and noise levels, producing intermediate
564 sizer-adder behavior for *A. thaliana* stem cells where $\alpha_g = -0.5, \sigma = 2$. If $\rho_{\mathrm{G2/M\ vs.G1/S}} \approx$
565 1, as is the case for mammalian cells (Cadart, 2018), apparent near-sizer behavior
566 between G1/S and G2/M ($l_{\mathrm{S/G2/M}} \approx 0$) is a key prediction (Fig. 7C, SI).
567
568 (2) A G1/S two-phase master regulator produced in proportion to growth with no gene-
569 copy number effect on regulator production ($\lambda_c = 1, r_{\mathrm{S/G2/M}} = 1$ in Eq. 1, $\alpha_{c,\mathrm{phase}} = -0.5$
570 (SI)) with a noisy, independently regulated S/G2/M such that $\eta_{\mathrm{G2/M}} \approx f_{\mathrm{S/G2/M}}/\sigma_{\mathrm{S/G2/M}}$.

571 Key predictions are supra-sizer S/G2/M control $f_{\mathrm{S/G2/M}} = l_{\mathrm{S/G2/M}} > 0$, $l_{\mathrm{G1}} \approx 0.5/l_{\mathrm{S/G2/M}}$

572 and $\rho_{\mathrm{G2/M\ vs.G1/S}} \approx 1.4\ \frac{l_{\mathrm{S/G2/M}}}{\sigma_{\mathrm{S/G2/M}}}$ (Fig. 7D).

573

574 (3) A G2/M two-phase master regulator produced with the same size dependence as

575 growth ($\lambda_c = 1$ in Eq. 2, $\alpha_{c,\mathrm{phase}} = -0.5$, SI), but, unlike growth, the regulator's

576 production rate is gene copy-number limited and doubles during S/G2/M ($r_{\mathrm{S/G2/M}} = 2$).

577 Key predictions are $l_{\mathrm{G1}} \approx 0$ and $l_{\mathrm{S/G2/M}} \approx 0.5$ (Fig. S3A).

578

579 (4) A G2/M two-phase master regulator produced in proportion to the square of cell size

580 throughout the cell cycle ($\lambda_c = 2$ in Eq. 2) with the same birth-size dependence as

581 growth and no gene copy-number effect ($\alpha_{c,\mathrm{phase}} = -0.5, r_{\mathrm{S/G2/M}} = 1$). Predictions are

582 similar to those of mechanism (1) (Fig. 7C vs. S3B), so it is necessary to measure

583 regulator dynamics to distinguish between mechanisms (1) and (4).

584

585 (5) A budding yeast-like G1/S inhibitor dilutor produced at a constant birth-size

586 independent rate through S/G2/M while S/G2/M exhibits timer regulation and a noisy

587 G1/S threshold concentration ($\eta_{\mathrm{G1/S}} \approx 0.7$ in Eq. 4). Predictions are $l_{\mathrm{G1}} \approx 0.4$, $l_{\mathrm{S/G2/M}} \approx$

588 1.2, and $\rho_{\mathrm{G2/M\ vs.G1/S}} \approx 1$ (Fig. S3C).

589

Discussion

Here, we developed a general, mechanistic model of cell proliferation with two cell cycle phases, aiming to achieve a pragmatic tradeoff between the representation of cell cycle complexity and model analyzability (Fig. 1). We applied the model to determine how size homeostasis is broken without necessarily disrupting the proper ordering of G1/S and G2/M or division by changing mechanisms of cell-cycle regulation (Fig. 2,3). For example, size homeostasis would break: (1) if the width of FtsZ bands were to increase proportionally with growth to trigger division at a local threshold density; (2) in slow-growing bacteria without multiple replication forks, if DnaA activity were to scale independently of or strongly with cell size while S/G2/M were under timer control; (3) in budding yeast, if Whi5 was produced in proportion to cell size rather than at a constant rate; (4) in many cases, with gene-copy number effects on regulator production. These findings reveal unintuitive constraints on cell-cycle regulation imposed by size homeostasis requirements. They explain why certain patterns of cell cycle regulation have been observed and not others, and suggest a breadth of cellular designs for the loss of size homeostasis, potentially enabling experimentalists to probe the physiological implications of a transient loss of size control.

General analytical expressions connect cell cycle control mechanisms to measured size homeostasis statistics (Eqs. 1-8, Methods, SI), thus providing a linchpin that ultimately

connects genotype to size-homeostasis phenotype. In some cases, unintuitive implications were revealed, such as the potential enhancement of adder behavior by noisy regulator production (Fig. 4), potential deviations from adder by regulator localization patterns (Fig. 5), and the curious statistical signatures of independently regulated phases (Fig. 6). We have inevitably approximated or omitted certain details of cell proliferation, yet the analytical expressions are a powerful basis for generating and testing hypotheses across a range of scenarios. To exemplify this power, we enumerated five mechanisms that account for the intermediate sizer-adder behavior between birth and division observed in *A. thaliana* apical stem cells with distinguishing predictions for other size-homeostasis statistics (Fig. 7). One plausible mechanism assumes CDK1-cyclin behaves as a master regulator triggering G2/M at a threshold level and is produced proportionally with cell size rather than growth rate throughout the cell cycle, thus implying that regulator production scales with bulk synthetic capacity of the cell (which presumably scales with size) rather than being directly coupled to growth. Then, if the CVs in cell size at G1/S and G2/M are similar, apparent near-sizer behavior over S/G2/M, corresponding to a zero correlation between G1/S size and G2/M size, is predicted (Fig. 7C). These predictions can be readily tested by quantitative time-lapse imaging of *A. thaliana* apical stem cells in strains containing extant G1/S and membrane reporters (Jones et al., 2017; Willis et al., 2016).

Why is adder behavior ubiquitous? Adder regulation may not be evolutionary advantageous *per se*, but may tend to result from evolutionary pressures on underlying regulator and growth dynamics with the necessity that catastrophic loss of size control is avoided. In fission yeast, widely conserved CDK-cyclin-like master regulators trigger multiple ordered events at successive threshold levels, operating as an "arrow of time" for the cell cycle (Swaffer et al., 2016). This ordering activity may generate pressures to degrade the regulator, thus preventing events in previous cell cycles from affecting future events, and to match the regulator production rate to the biosynthetic capacity of the cell to ensure events occur only when cellular machineries are sufficiently plentiful. Then, events are necessarily triggered at a threshold level rather than concentration to avoid a loss of size control and, for regulators of DNA replication initiation which persist between intervening divisions such as active DnaA, size-homeostasis robustness precludes a production rate that deviates strongly from being proportional to growth. These mechanisms result in apparent adder behavior between birth and division without implementing a "molecular adder" that specifically effects a fixed added-size increment. The use of cell size statistics alone to conclude "molecular adders" may lead to incorrect inferences about the basis of cell-cycle regulation, recalling flawed conclusions about intrinsic noise derived from a dual reporter system (Hilfinger and Paulsson, 2011). In slow growing cells where the constraints on the timing of events may be relatively relaxed, deviations from these mechanisms and thus from adder

behavior may arise. Alternatively, adder regulation of S/G2/M may be advantageous in conferring a robustness to size control against variations in other cell proliferation factors (Fig. 2A, 3A-C), especially the dynamics of G1/S regulation; in many conditions and organisms, G1/S occurs shortly after G2/M or division, so the observed adder regulation between birth and division may be generated by S/G2/M adder regulation.

In general, our findings exemplify how the model combined with quantitative time-lapse measurements of cell size dynamics and cell cycle reporters across species, mutants, and conditions should not only help to establish the mechanisms of cell cycle regulation, but further illuminate their necessity for size control. Such a fundamental understanding will inform whether the frequently observed adder behavior emerges from a common mechanism, is a product of convergent evolution due to selective pressures on size homeostasis, or is merely a manifestation of specific regimes of mechanisms without molecular adders that happened to have been the focus of experiments thus far. The intimate connections between size control and other cellular processes should also be an important factor in probing the response of cells to non-steady-state conditions and to the future design of artificial cells.

667 **Acknowledgements**

668 The authors thank members of the Huang Laboratory and Clotilde Cadart, Po-Yi Ho,
669 Benjamin Knapp, and Fred Chang for helpful discussions. This work was supported by
670 the Allen Discovery Center at Stanford on Systems Modeling of Infection (to K.C.H.)
671 and the Gatsby Charitable Foundation under Grant GAT3395/PR4 (to H.J.). K.C.H. is a
672 Chan Zuckerberg Biohub Investigator. This work was also supported in part by the
673 National Science Foundation under Grant PHYS-1066293 (to K.C.H.) and the hospitality
674 of the Aspen Center for Physics.

675

676 **Author Contributions**

677 Conceptualization, L.W., H.J., and K.C.H.; Methodology, L.W. and K.C.H.; Formal
678 analysis, L.W.; Writing-Original draft, L.W. and K.C.H.; Writing-Review and editing,
679 L.W., H.J., and K.C.H.; Funding acquisition, L.W., H.J., and K.C.H.

680

681 **Declarations of Interests**

682 The authors declare no competing interests.

683

Figure Legends

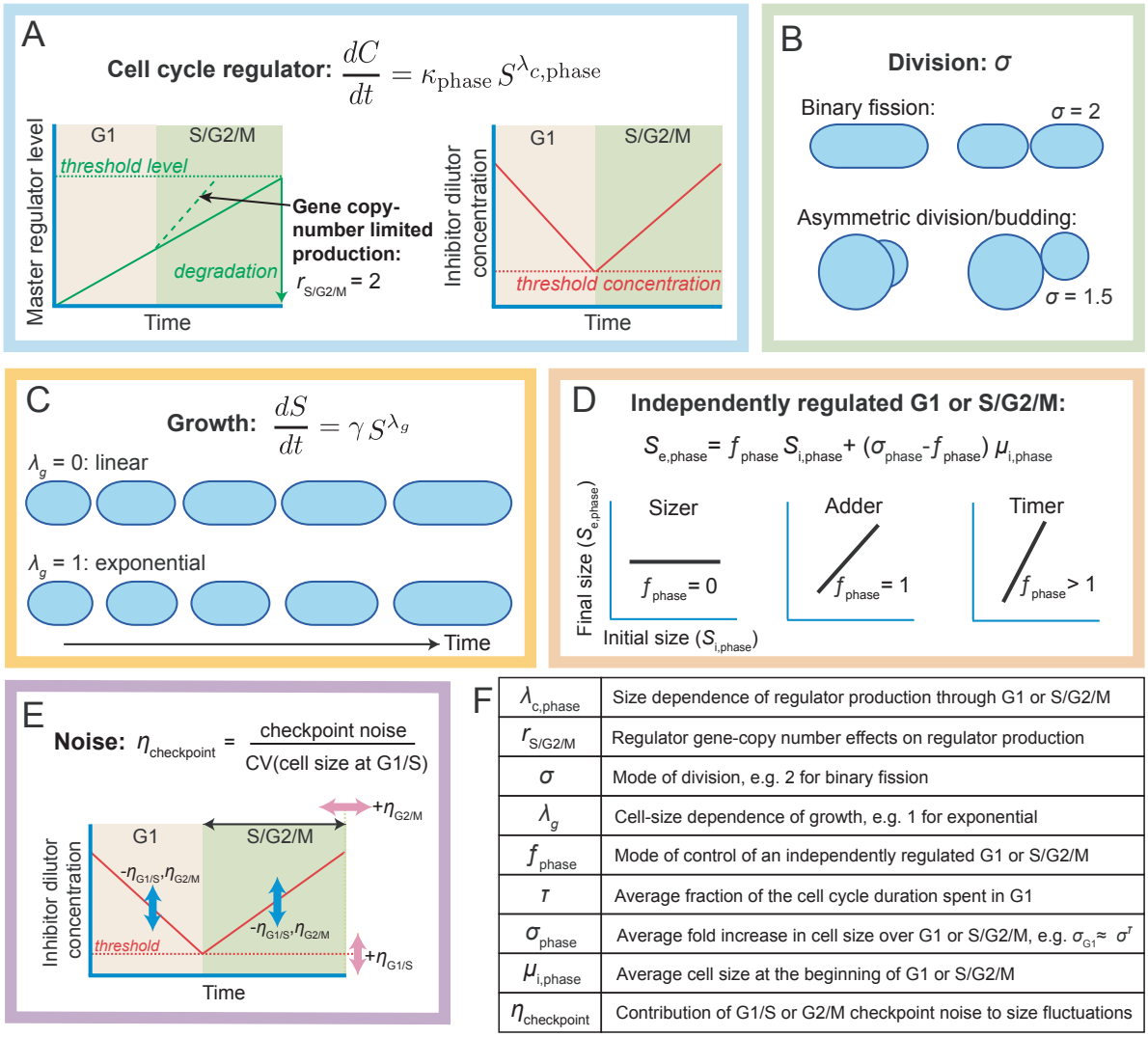

$\lambda_{c,\text{phase}}$	Size dependence of regulator production through G1 or S/G2/M
$r_{S/G2/M}$	Regulator gene-copy number effects on regulator production
σ	Mode of division, e.g. 2 for binary fission
λ_g	Cell-size dependence of growth, e.g. 1 for exponential
f_{phase}	Mode of control of an independently regulated G1 or S/G2/M
τ	Average fraction of the cell cycle duration spent in G1
σ_{phase}	Average fold increase in cell size over G1 or S/G2/M, e.g. $\sigma_{G1} \approx \sigma^{\tau}$
$\mu_{i,\text{phase}}$	Average cell size at the beginning of G1 or S/G2/M
$\eta_{\text{checkpoint}}$	Contribution of G1/S or G2/M checkpoint noise to size fluctuations

Figure 1: A general model of cell proliferation with two cell-cycle checkpoints.

(A)The dependence of cell-cycle regulator production rate $\left(\frac{dC}{dt}\right)$ on cell size (S) is dictated by $\lambda_{c,\text{phase}}$, with the phase corresponding to either G1 or S/G2/M. $\lambda_{c,\text{phase}} = 1$ corresponds to size-proportional production. Master regulators (left) are produced throughout one or both phases at a rate that may increase with

692 gene-copy number (corresponding to $r_{\mathrm{S/G2/M}} = \kappa_{\mathrm{S/G2/M}}/\kappa_{\mathrm{G1}} = 2$) to trigger G1/S
693 or G2/M at a threshold total intracellular level, and then are degraded. Inhibitor
694 dilutors (right) are produced throughout one phase only ($\kappa_{\mathrm{G1}} = 0$) and then
695 diluted out in the next, triggering G1/S or G2/M at a threshold concentration.
696 (B) Cell division may occur through binary fission ($\sigma = 2$) or asymmetrically ($\sigma < 2$
697 or $\sigma > 2$).
698 (C) Cell growth is exponential, linear, or intermediate ($\lambda_g = 1, 0$, or otherwise,
699 respectively).
700 (D) Cell cycle regulators can operate in combination with an independently
701 regulated G1 or S/G2/M phase, meaning that the size at the end of the phase
702 ($S_{\mathrm{e,phase}}$) depends only on the size at the beginning of the phase ($S_{\mathrm{i,phase}}$) and not
703 on prior sizes, with the mode of regulation dictated by f_{phase}: $f_{\mathrm{phase}} = 0, 1$ or
704 depends on the growth behavior for critical size ("sizer"), adder, or timer
705 regulation, respectively. σ_{phase} is the steady state average fold increase in cell size
706 over the phase; $\sigma_{\mathrm{G1}} \approx \sigma^{\tau}$, where τ is the fraction of the cell cycle taken up by G1,
707 and $\sigma_{\mathrm{S/G2/M}} \approx \sigma^{1-\tau}$. The average initial size $\mu_{\mathrm{i,phase}}$ can be expressed in terms of
708 other model parameters (Table S1, SI).
709 (E) Cell-size fluctuations are due to noise in regulator dynamics and cell-cycle
710 checkpoints. Noise effects are summarized by $\eta_{\mathrm{G1/S}}$ and $\eta_{\mathrm{G2/M}}$, corresponding to
711 the noise in the G1/S and G2/M checkpoint criteria, respectively, divided by the

coefficient of variation (CV) in G1/S size. For example, the G2/M checkpoint noise of S/G2/M timer control is generated by noise in the fixed time period between G1/S and G2/M (horizontal pink arrow); for G1/S inhibitor dilutors, noise in the minimum threshold concentration generates the G1/S checkpoint noise (vertical pink arrow). Noise sources that increase CV(cell size at G1/S) without affecting noise in the checkpoint criteria, for example noise in the production or dilution of the inhibitor (blue arrows), reduce $\eta_{\mathrm{G1/S}}$ and $\eta_{\mathrm{G2/M}}$.

(F) Definitions of key parameters determining size-homeostasis behaviors.

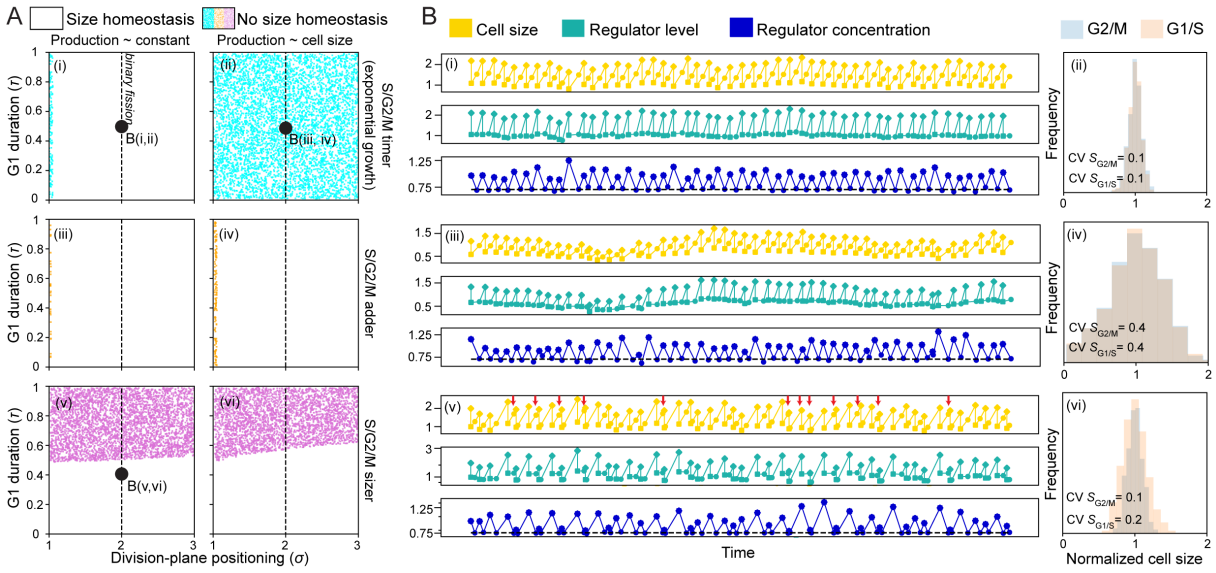

720

721 **Figure 2: G1/S inhibitor dilutors combined with S/G2/M sizer or timer regulation can**

722 **fail to achieve size homeostasis.**

723 (A) Colored regions indicate where G1/S size homeostasis is lost (as defined by

724 analytical results for exponentially growing cells ($\lambda_g = 1$) with G1/S inhibitor-

725 dilution control in which the absolute value of the slope of G1/S size in

726 generation n vs. generation n+1 is >0.95) for a range of division-plane positions

727 (σ; x-axis), G1 durations (τ; y-axis), different modes of S/G2/M regulation (rows),

728 and inhibitor production being constant (left) or proportional to cell size (right).

729 If S/G2/M is under timer regulation, size homeostasis is predicted to be achieved

730 if production is not size-dependent ($\lambda_{c,\mathrm{S/G2/M}} = 0$) (i) but generally lost if

731 inhibitor production is proportional to cell size ($\lambda_{c,\mathrm{S/G2/M}} = 1$) (ii). Regardless of

732 growth and production patterns, G1/S inhibitor dilutors are also predicted to be

733 incompatible with the combination of G2/M sizer regulation and long G1

734 durations ($\tau \geq 0.5$) (v,vi). S/G2/M adder regulation generally maintains size
735 homeostasis (iii,iv). Black ccircles correspond to single cell lineages simulated in
736 (B).
737 (B) Simulations of single cell lineages with realistic noise levels confirm analytical
738 results. (i,ii) Cell size, inhibitor level, and inhibitor concentration control are
739 achieved for a budding yeast-like inhibitor dilutor ($\lambda_{c,\mathrm{S/G2/M}} = 0, \sigma = 2, \tau = 0.5$)
740 in exponentially growing cells ($\lambda_g = 1$) with S/G2/M timer regulation and
741 realistic noise levels (coefficient of variation (CV) of G2/M size ≈ 0.1, produced
742 by noise terms $\xi_{\mathrm{C,G1}}, \xi_{\mathrm{C,S/G2/M}}, \xi_{\mathrm{G1/S}}, \xi_{\mathrm{G2/M}} = 0.03$, Methods), as demonstrated by a
743 cell lineage (left) and the corresponding G1/S and G2/M size distributions (right).
744 In the cell lineage, squares, circles, and diamonds denote birth, G1/S, and G2/M
745 (division), respectively. (iii, iv) For the same noise levels as in (i,ii), cell-size
746 control was nearly lost when the inhibitor's production was $\lambda_{c,\mathrm{S/G2/M}} = 0.95 \approx$
747 $\lambda_g = 1$ (the same size dependence as growth). The size distributions (iv) show
748 that transitions frequently occur at ~10% or ~200% of the usual size. (v,vi) G2/M
749 sizer control causes loss of G1/S size homeostasis if the G1 duration is long ($\sigma =$
750 $2, \tau = 0.4$ are at the boundary of G1/S size homeostasis, as indicated in Fig. 2A(v);
751 CV of G2/M size ≈ 0.1, produced by $\xi_{\mathrm{C,G1}}, \xi_{\mathrm{C,S/G2/M}}, \xi_{\mathrm{G1/S}} = 0.01, \xi_{\mathrm{G2/M}} = 0.1$,
752 Methods). Red arrows point to cell cycles where G1/S occurred near the end of
753 the cell cycle; in the following cell cycle, G1/S tends to occur early. The G1/S size

754 distribution (vi) shows G1/S frequently occurs at ~60% or ~140% of the average

755 G1/S size, and therefore at ~0.6 $\sigma_{G1} = 0.6\ 2^{\tau} = 0.8$ or ~1.4 $\sigma_{G1} = 1.4\ 2^{\tau} = 1.8$ of the

756 average birth size.

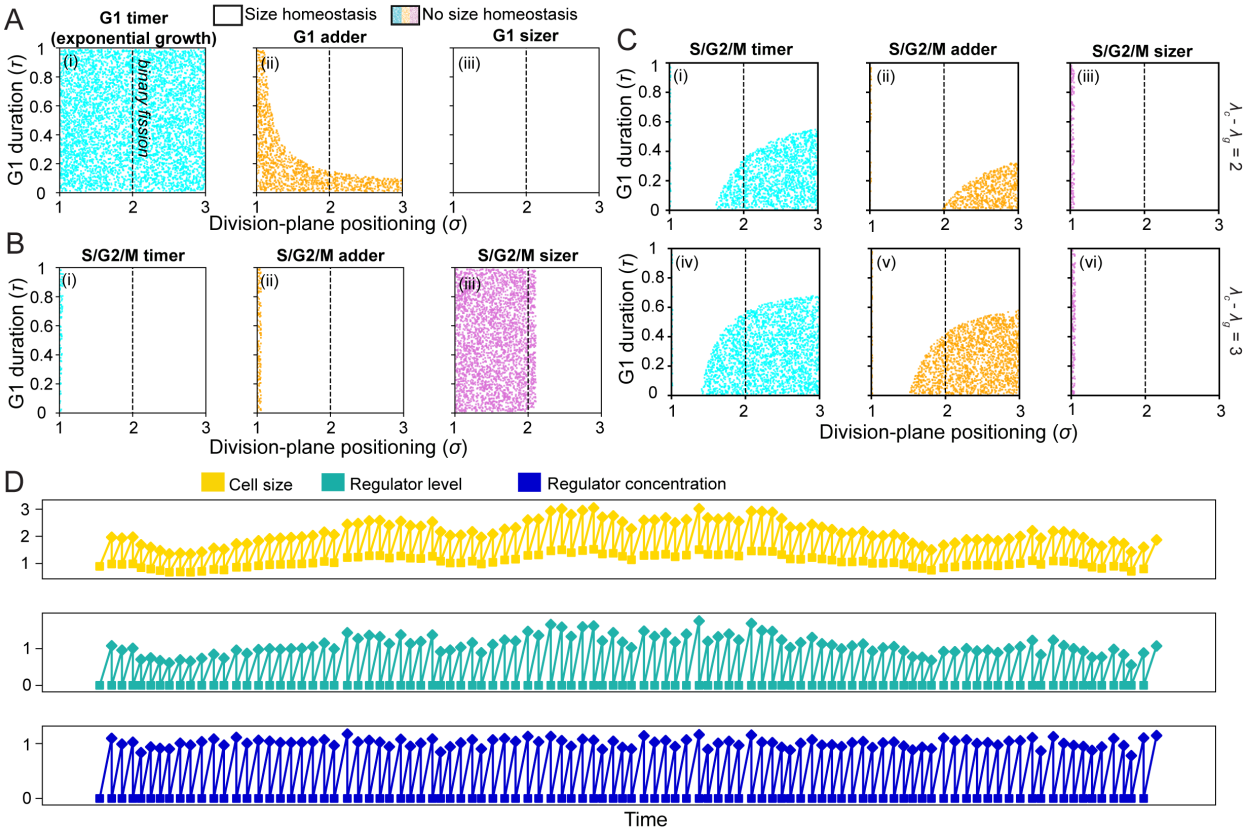

Figure 3: Master regulators can lose cell-size control when production is gene copy-number limited or strongly size-dependent, or a threshold concentration rather than level triggers phase progression.

(A)G2/M two-phase master regulators with size-independent production rates ($\lambda_{c,\mathrm{G1}} = \lambda_{c,\mathrm{S/G2/M}} = 0$) can achieve cell-size regulation in exponentially growing cells ($\lambda_g = 1$) if their production rate is gene copy-number limited ($r_{\mathrm{S/G2/M}} = 2$) while G1 is under sizer (iii) or adder (ii) regulation, but not timer regulation (i). Colored regions indicate parameters in which G2/M size homeostasis is lost.

(B) G1/S two-phase master regulators with gene copy-number limited production

767 that have the same size-dependencies as growth ($\lambda_{c,\mathrm{G1}} = \lambda_{c,\mathrm{S/G2/M}} = \lambda_g$) achieve
768 size homeostasis for S/G2/M adder (ii) and timer (i) regulation, but are
769 incompatible with G2/M sizer regulation when $\sigma \leq 2$ (iii). Colored regions
770 indicate parameters in which G1/S size homeostasis is lost.
771 (C) G1/S two-phase master regulators with strongly size-dependent production ($\lambda_c -$
772 $\lambda_g = 2$ (top) or 3 (bottom) where $\lambda_c = \lambda_{c,\mathrm{G1}} = \lambda_{c,\mathrm{S/G2/M}}$) and no gene-copy
773 number effects fail to achieve size homeostasis for S/G2/M timer (i,iv) and adder
774 (ii,v) regulation for long S/G2/M durations ($1 - \tau > 0.5$) and binary fission ($\sigma \geq$
775 2). Colored regions indicate parameters in which G1/S size homeostasis is lost.
776 (D) The size (i), regulator level (ii), and regulator concentration (iii) trajectories of a
777 cell lineage governed by a two-phase master regulator that is produced from an
778 initial level of zero and triggers G2/M at a noisy threshold concentration instead
779 of a noisy threshold total intracellular level, with size-dependent production
780 $\lambda_c = \lambda_{c,\mathrm{G1}} = \lambda_{c,\mathrm{S/G2/M}} = 1.05$ similar to the size-dependence of growth $\lambda_g = 1$.
781 Cell size fluctuates dramatically as λ_c approaches λ_g, and size control is lost in
782 the limit that $\lambda_c = \lambda_g$. Squares and diamonds denote birth and G2/M (division),
783 respectively.

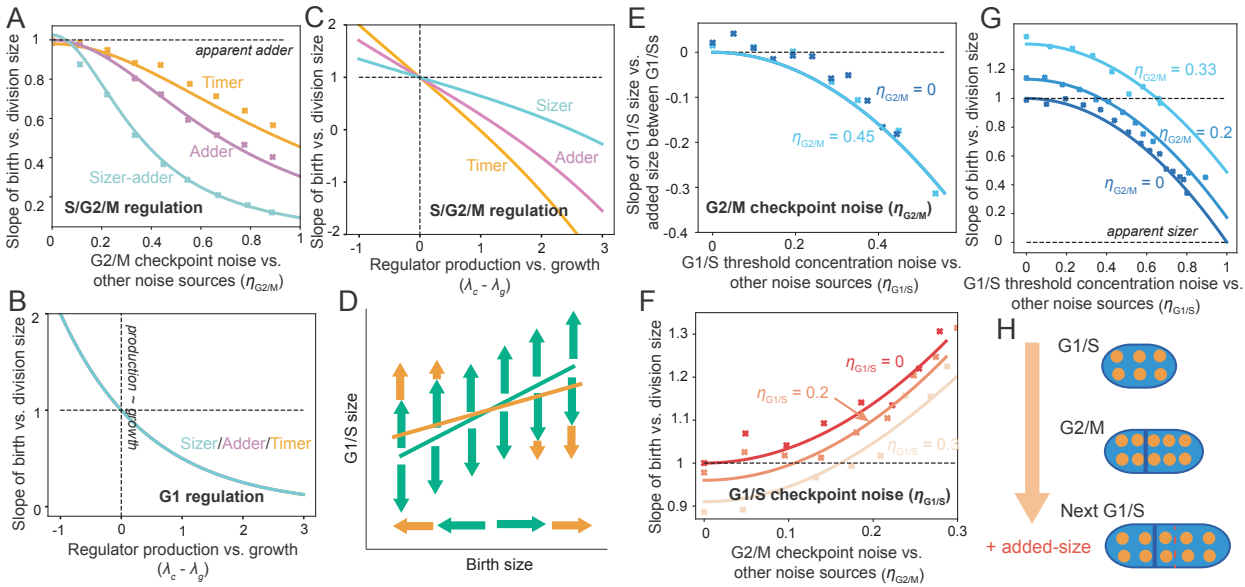

784

785 **Figure 4: Cell-cycle regulation mechanisms can produce various apparent size**

786 **homeostasis behaviors depending on factors such as noise and regulator production.**

787 (A)G1/S two-phase master regulators that are produced in proportion to growth

788 ($\lambda_c = \lambda_g$, $r_{\mathrm{S/G2/M}} = 1$ in Eq. 1) exhibit a linear regression slope of ~1 between

789 birth and division regardless of the S/G2/M regulatory mode, representing

790 apparent adder behavior, as long as the G2/M checkpoint makes a weak

791 contribution to size fluctuations ($\eta_{\mathrm{G2/M}} \ll 1$). Analytical approximations (solid

792 lines, SI) agree with exact simulations (symbols) for realistic noise levels (CV of

793 G1/S size ≈ CV of G2/M size ≈ 0.1). In the plots, $\sigma_{\mathrm{S/G2/M}} = 1.4$ was assumed.

794 (B) G2/M two-phase master regulators produce slopes ~0 and thus near-sizer

795 behaviors when production is strongly size-dependent with no gene copy-

796 number effects ($\lambda_c > \lambda_g$, $r_{\mathrm{S/G2/M}} = 1$ in Eq. 2) regardless of the G1 regulatory

mode (the curves for G1 timer, adder, and sizer regulation are all identical) and noise levels. Here, binary fission ($\sigma = 2$) was assumed.

(C) By contrast, G1/S two-phase master regulators tend to produce negative slopes for strongly size-dependent production with no gene copy-number effects ($\lambda_c > \lambda_g$, $r_{\mathrm{S/G2/M}} = 1$ in Eq. 1). Here, weak G2/M checkpoint noise ($\eta_{\mathrm{G2/M}} \ll 1$), $\sigma_{\mathrm{S/G2/M}} = 1.4$, and $\sigma = 2$ were assumed.

(D) Among G1/S two-phase master regulators, relatively high noise in the G2/M checkpoint mechanism results in small or large cells at birth with low or high regulator levels, respectively. Small cells then grow more and thus produce more regulator to achieve the surplus regulator level for G1/S progression (orange arrows). Noise sources that impact the regulator's production are uncoupled from initial birth size, and thus do not affect the size homeostasis behavior between birth and G1/S (green arrows).

(E-G) Depending on which processes make the largest contributions to cell-size fluctuations, a budding yeast-like G1/S inhibitor-dilutor with S/G2/M timer regulation can generate a variety of size homeostasis behaviors as represented by the linear regression slopes among size variables: if noise in inhibitor dynamics primarily generates G1/S size fluctuations ($\eta_{\mathrm{G1/S}} \ll 1$, $\eta_{\mathrm{G2/M}} \ll 1$ in Eq. 4), apparent adder behavior results between consecutive G1/Ss (E) and birth and division (F,G). $\eta_{\mathrm{G1/S}} \ll 1$ requires stringent control of G1/S.

817 (H) Addition of a constant amount of inhibitor (orange spots) over S/G2/M achieves
818 adder size homeostasis between consecutive G1/Ss, because added size scales
819 with amount of inhibitor produced owing to the threshold inhibitor
820 concentration requirement for G1/S progression.

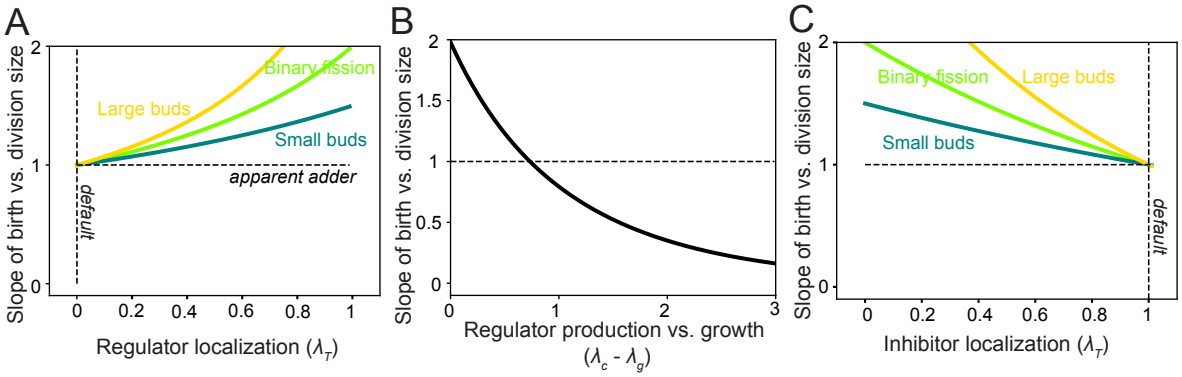

Figure 5: Deviations in regulator localization patterns cause supra-adder behaviors.

(A) G2/M two-phase master regulators that localize to a region that scales with cell size as S^{λ_T} to trigger checkpoint progression at a threshold density produce a slope between birth and division size of $\frac{1}{1-\lambda_T(1-\sigma^{-1})}$, generating supra-adder behavior as λ_T deviates from zero (the model's default scenario), assuming regulator production is proportional to growth ($\lambda_g = \lambda_c$ in Eq. 5). (Yellow, light green, or dark green lines are for $\sigma = 3, 2$, or 1.5).

(B) For a G2/M threshold concentration rather than threshold level, the slope between birth and division size is $\frac{1+\Delta\lambda}{\sigma^{-1}+\Delta\lambda\sigma^{\Delta\lambda}}$ where $\Delta\lambda = \lambda_c - \lambda_g$ (assuming $r_{\mathrm{S/G2/M}} = 1$), which gives adder behavior when $\Delta\lambda \approx 0.7$ for binary fission (σ =2).

(C) Budding yeast-like G1/S inhibitor dilutors that localize to a region that scales with cell size as S^{λ_T} to trigger phase progression at a threshold density produce a slope between birth and division size of $\sigma^{1-\lambda_T}$, generating supra-adder behavior as λ_T deviates from one (the model's default scenario), assuming a fixed average amount of inhibitor is produced during S/G2/M and noisy

inhibitor dynamics ($\eta_{\mathrm{G1/S}}, \eta_{\mathrm{G2/M}} \ll 1$ in Eq. 6). (Yellow, light green, or dark green lines are for $\sigma = 3, 2$, or 1.5, respectively).

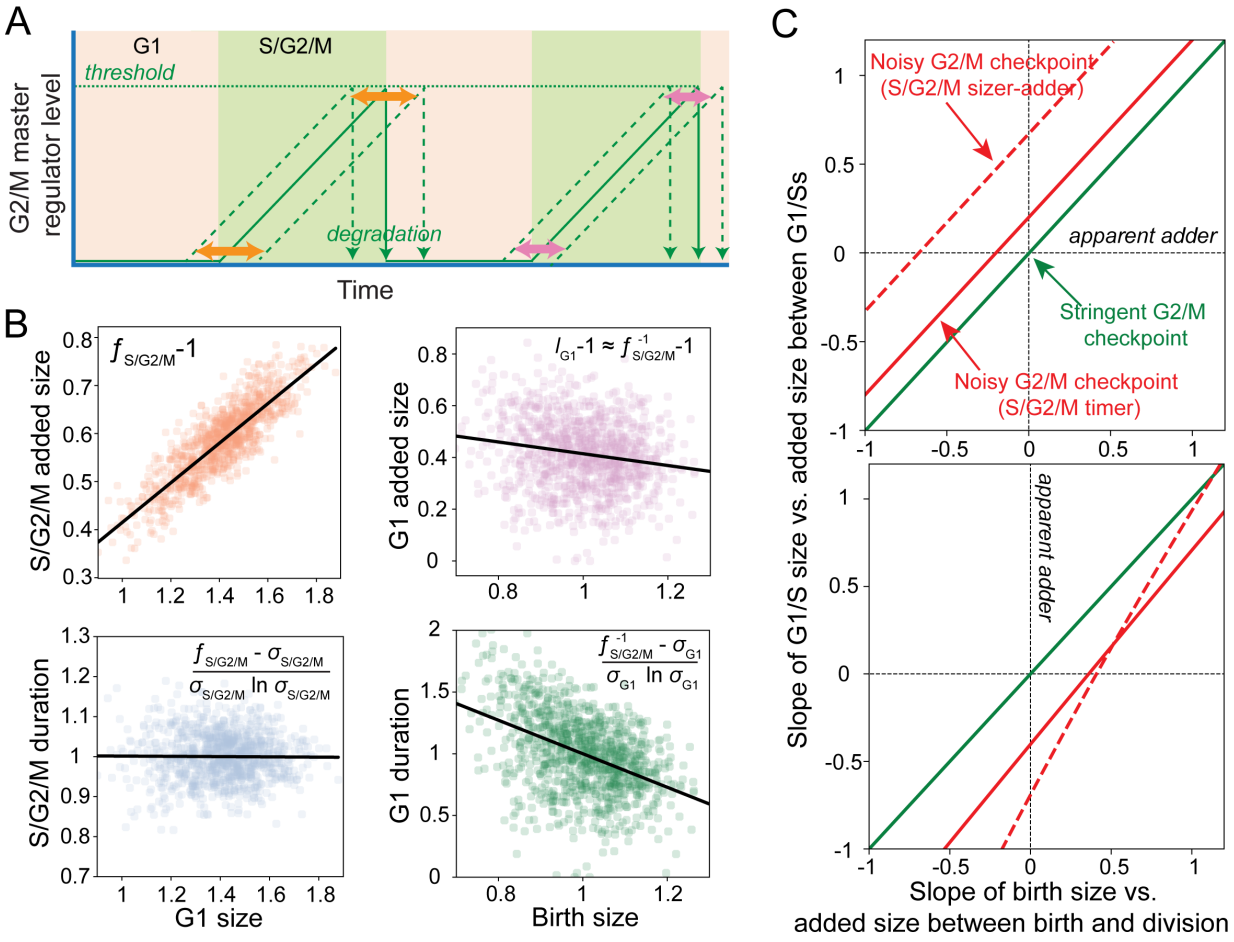

Figure 6: Apparent adder regulation between birth and division with non-adder regulation over G1 and S/G2/M can be achieved by independently regulated G1/S and G2/M transitions.

(A) In independently regulated phases, size fluctuations (orange and pink) depend on events during but not prior to that phase. If G2/M is triggered by a cyclin-like master regulator that accumulates only through S/G2/M and is degraded outside of this phase, then S/G2/M is likely to be independently regulated from G1.

(B) Simulations demonstrate a compensatory behavior in which the size added during G1 offsets the opposite trend over S/G2/M. This behavior is naturally achieved by control mechanisms that give apparent adder behavior between birth and division combined with an independently regulated phase. Panels: Simulated scatter plots of size-homeostasis statistics for a budding yeast-like G1/S inhibitor dilutor with low checkpoint noise ($\eta_{\mathrm{G1/S}}, \eta_{\mathrm{G2/M}} \ll 1$ in Eq. 4) and the corresponding analytical expressions for the linear regression slopes (SI). Noise terms: $\xi_{\mathrm{C,G1}}, \xi_{\mathrm{C,S/G2/M}} = 0.05, \xi_{\mathrm{G1/S}}, \xi_{\mathrm{G2/M}} = 0.02$ give realistic size fluctuations CV of G1/S size ≈ CV of G2/M size ≈ 0.1.

(C) The apparent size-homeostasis behaviors between consecutive G2/Ms and consecutive G1/Ss are identical if the cell cycle is controlled by one independently regulated phase with low checkpoint noise (either G1/S or G2/M). Top: For a G1/S two-phase master regulator combined with an independently regulated S/G2/M phase and realistic noise levels (CV of G1/S size ≈ 0.1), the same size-homeostasis behavior is observed between birth and division and consecutive G1/Ss when the G2/M checkpoint is stringent (green line); the equality is lost as G2/M checkpoint noise contributions increases (red lines). Different size homeostasis behaviors were achieved by varying the size dependency of the regulator's production rate (λ_c). Bottom: results are similar for

866 G1/S inhibitor dilutors combined with an independently regulated S/G2/M

867 phase.

A

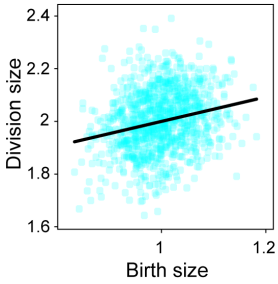

B

Mechanism	Ref.	Predicted l_{G1}	Predicted $l_{S/G2/M}$	Predicted $\rho_{G1\ vs.\ S/G2/M}$
(1) G2/M two-phase master regulator with no birth-size dependent production	Eq. 8, Fig. 7C	No restriction	$-0.3 + 0.4\ l_{G1}(\rho_{G1\ vs.\ S/G2/M})^2$	No restriction
(2) G1/S two-phase master regulator with a noisy G2/M checkpoint	Eq. 1, Fig. 4A, 7D	$0.5/l_{S/G2/M}$	>0	$1.4\ l_{S/G2/M}/\sigma_{S/G2/M}$
(3) G2/M two-phase master regulator with gene copy-number limited production	Eq. 2, Fig. S3A	0	0.5	No restriction
(4) G2/M two-phase master regulator with production ~cell-size squared	Eq. 2, Fig. 4B, S3B	No restriction	$l_{G1}(\rho_{G1\ vs.\ S/G2/M})^2/4$	No restriction
(5) G1/S budding yeast-like inhibitor dilutor with a noisy G1/S checkpoint	Eq. 4, Fig. 4G, S3C	0.4	1.2	1

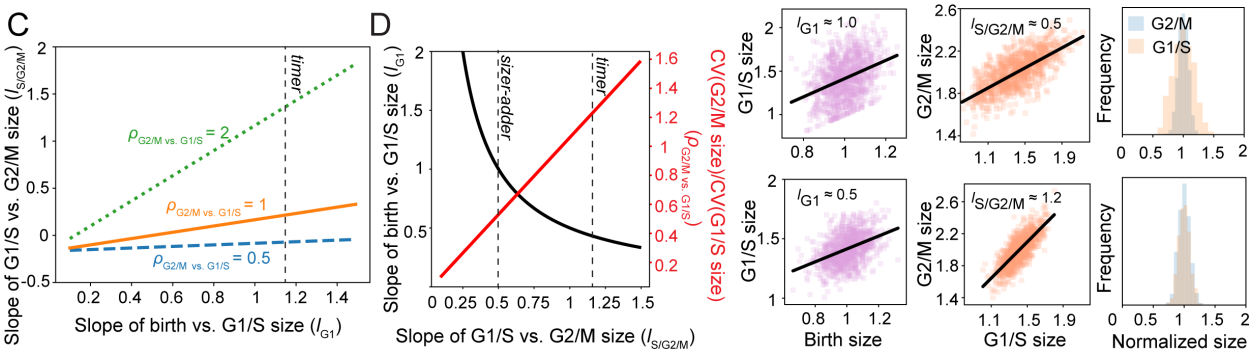

868

869 **Figure 7: Extended size-homeostasis statistics can discriminate among different**

870 **possible mechanisms underlying intermediate sizer-adder behavior.**

871 All simulations are based on realistic noise levels ($\rho_{G1/S} \approx \rho_{G2/M} \approx 0.1$). Solid black

872 lines in scatter plots correspond to linear regression fits.

873 (A) A linear regression slope of ≈ 0.5 between birth and division sizes corresponds

874 to the intermediate sizer-adder behavior identified in *A. thaliana* stem cells.

875 (B) A summary of mechanisms (1)—(5) and the relevant equations and figures that

876 generate intermediate sizer-adder behavior, in some cases with distinguishing

877 predictions for the linear regression slopes between birth and G1/S sizes (l_{G1}) and

878 G1/S and G2/M sizes ($l_{S/G2/M}$), and the ratio of the CVs in G2/M size vs. G1/S size

879 ($\rho_{G2/M\ vs.G1/S}$).

(C) Mechanism 1: A G2/M two-phase master regulator produced in proportion to cell size with no birth-size or gene copy-number. Predictions for $l_{\mathrm{S/G2/M}}$ depend on l_{G1} and $\rho_{\mathrm{G2/M\ vs.\ G1/S}}$: there is apparent near-sizer behavior over S/G2/M ($l_{\mathrm{S/G2/M}} \approx 0.0$) if the CV in G1/S size exceeds or equals that of G2/M size ($\rho_{\mathrm{G2/M\ vs.\ G1/S}} \leq 1$).

(D) Mechanism 2: A G1/S two-phase master regulator produced in proportion to growth with noisy supra-sizer S/G2/M regulation such that $\eta_{\mathrm{G2/M}} \approx f_{\mathrm{S/G2/M}}/\sigma_{\mathrm{S/G2/M}}$. Different modes of independently regulated S/G2/M control ($f_{\mathrm{S/G2/M}} = l_{\mathrm{S/G2/M}}$) predict different l_{G1}s and $\rho_{\mathrm{G2/M\ vs.\ G1/S}}$ (left); for example, S/G/M intermediate sizer-adder vs. timer regulation ($l_{\mathrm{S/G2/M}} = 0.5$ vs. $l_{\mathrm{S/G2/M}} = 1.2$) predict $l_{\mathrm{G1}} \approx 1.0$ and $\rho_{\mathrm{G2/M\ vs.\ G1/S}} \approx 0.6$ (right, top row) vs. $l_{\mathrm{G1}} \approx 0.5$ and $\rho_{\mathrm{G2/M\ vs.\ G1/S}} \approx 1.5$ (right, bottom row), respectively. In the simulations, noise terms $\xi_{\mathrm{C,G1}}, \xi_{\mathrm{C,S/G2/M}}, \xi_{\mathrm{G1/S}} = 0.12; \xi_{\mathrm{G2/M}} = 0.06$ (top); $\xi_{\mathrm{C,G1}}, \xi_{\mathrm{C,S/G2/M}}, \xi_{\mathrm{G1/S}}, \xi_{\mathrm{G2/M}} = 0.06$ (bottom) produce realistic CVs of cell size ≈ 0.1. Mechanisms (3—5) in panel (B) are represented in Fig. S3.

Supplemental Figures

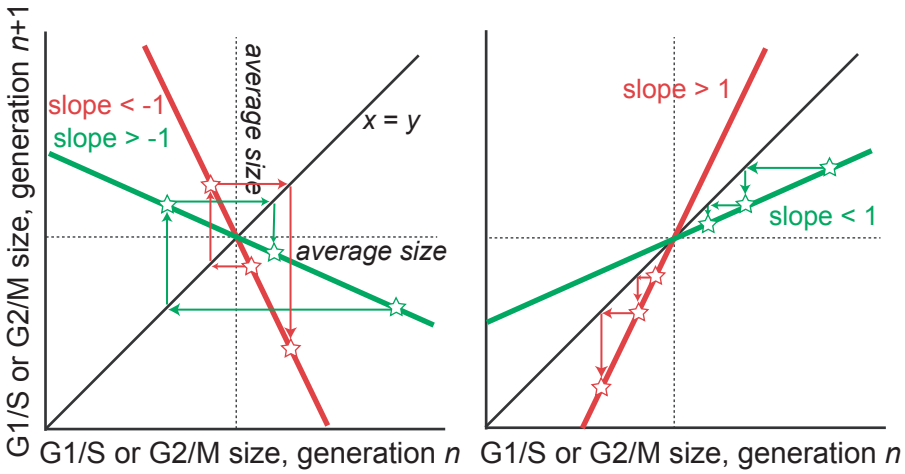

Figure S1: Conditions for loss of cell-size homeostasis. Related to Figures 2 and 3. For cells to achieve control of G1/S or G2/M size, the linearized relationship between cell sizes at G1/S or G2/M in consecutive cell cycles must have a slope between -1 and 1 (green trajectories). Size fluctuations then regress to the average, as opposed to diverging (red trajectories).

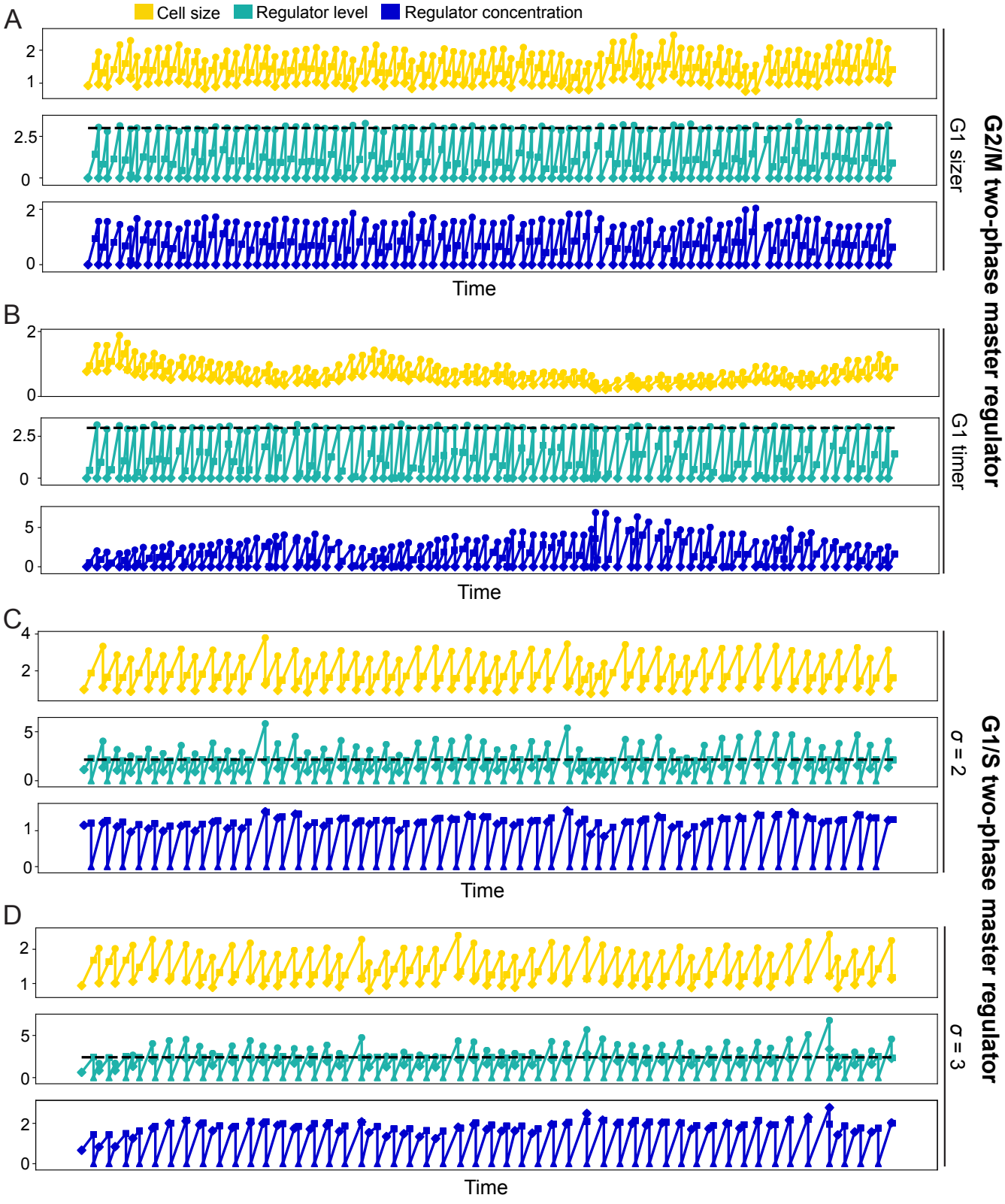

Figure S2: Simulations of single-cell lineage trajectories support analytical findings. Related to Figure 3. G2/M and G1/S master regulators produced through both phases (two-phase master regulators) fail to implement size homeostasis under certain conditions.

(A,B) For exponentially growing cells ($\lambda_g = 1$), when regulator production is gene copy-number limited ($r_{\mathrm{S/G2/M}} = 2$), G2/M two-phase master regulators produced at a size-independent rate ($\lambda_{c,\mathrm{G1/S}} = \lambda_{c,\mathrm{S/G2/M}} = 0$) achieve size homeostasis for G1 critical size or adder control regardless of the average G1 duration (τ), but fail to achieve size homeostasis for G1 timer control (Fig. 3A, Table S2). (A) shows size and regulator level homeostasis for G1 critical size regulation ($f_{\mathrm{G1}} = 0$, τ = 0.5, $\sigma = 2$; noise terms $\xi_{\mathrm{C,G1}}, \xi_{\mathrm{C,S/G2/M}} = 0.05$, $\xi_{\mathrm{G1/S}}, \xi_{\mathrm{G2/M}} = 0.1$ produce a CV of cell size ≈ 0.1); (B) shows the loss of homeostasis when G1 control approaches timer ($f_{\mathrm{G1}} = 0.99\,\sigma^{\tau}$) while other parameters remain fixed. Diamonds, squares, and discs denote values at birth, G1/S, and G2/M or division, respectively.

(C,D) G1/S two-phase master regulators that are gene copy-number limited fail to implement G1/S size homeostasis when combined with G2/M sizer regulation ($f_{\mathrm{S/G2/M}} = 0$) for binary fission or asymmetric division with $\sigma \leq 2$, regardless of G1 duration, the size dependence of regulator production, and growth pattern (Fig. 3B, Table S2); (C) shows size homeostasis for gene copy-number limited ($r_{\mathrm{S/G2/M}} = 2$) G1/S two-phase master regulators when $\sigma = 3$ (τ = 0.5, linear

924 growth pattern $\lambda_g = 0$; regulator production $\lambda_{c,\mathrm{G1/S}} = \lambda_{c,\mathrm{S/G2/M}} = 0$; and noise
925 terms $\xi_{\mathrm{C,G1}}, \xi_{\mathrm{C,S/G2/M}}, \xi_{\mathrm{G1/S}} = 0.02, \xi_{\mathrm{G2/M}} = 0.1$ producing a CV of cell size ≈ 0.1);
926 (D) shows the loss of G1/S size homeostasis when $\sigma = 2$ while other parameters
927 remain fixed. Diamonds, squares, triangles, and discs denote values at birth,
928 G1/S, immediately after G1/S when the regulator is degraded, and G2/M or
929 division, respectively. Horizontal dashed lines show the threshold regulator level
930 triggering phase progression.

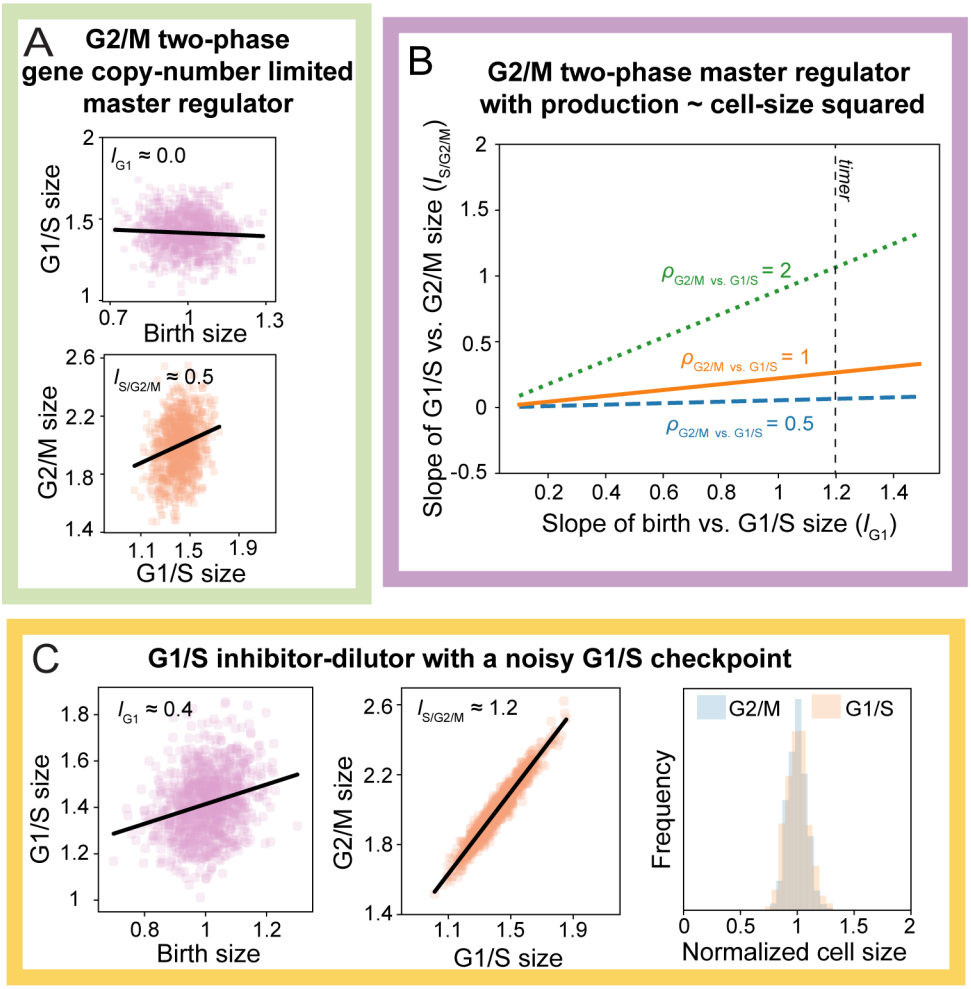

931

932 **Figure S3: Extended size-homeostasis statistics can discriminate among different**

933 **possible mechanisms underlying intermediate sizer-adder behavior.** Related to Figure

934 7; the panels represent mechanisms (3-5) listed in Fig. 7B. In all simulations, noise terms

935 were set to produce realistic CVs of cell size ≈ 0.1.

936 (A)Mechanism 3: A G2/M two-phase master regulator produced in proportion to

937 cell size ($\lambda_{c,\mathrm{phase}} = 1$) with the same birth-size dependence as growth ($\alpha_{c,\mathrm{phase}} =$

938 -0.5) (SI) and gene copy-number limited production ($r_{\mathrm{S/G2/M}} = 2$), with the latter
939 implying that regulator production is not proportional to growth throughout the
940 cell cycle. Predictions are G1/S sizer regulation ($l_{\mathrm{G1}} \approx 0$; top) and apparent sizer-
941 adder regulation over S/G2/M ($l_{\mathrm{S/G2/M}} \approx 0.5$; bottom). In the simulation, noise
942 terms were $\xi_{\mathrm{C,G1}}, \xi_{\mathrm{C,S/G2/M}}, \xi_{\mathrm{G1/S}}, \xi_{\mathrm{G2/M}} = 0.08$.

943 (B) Mechanism 4: A G2/M two-phase master regulator produced in proportion to
944 cell-size squared ($\lambda_{c,\mathrm{G1}} = \lambda_{c,\mathrm{S/G2/M}} = 2$) with no gene copy-number effect
945 ($r_{\mathrm{S/G2/M}} = 1$) and the same birth-size dependence as growth ($\alpha_{c,\mathrm{G1}} = \alpha_{c,\mathrm{S/G2/M}} =$
946 -0.5) (SI). Predictions are similar to mechanism (1) (Fig. 7C).

947 (C) Mechanism 5: A G1/S budding yeast-like inhibitor-dilutor with high G1/S
948 checkpoint noise. Further predictions are intermediate sizer-adder behavior over
949 G1 ($l_{\mathrm{G1}} \approx 0.4$), apparent near adder behavior over S/G2/M ($l_{\mathrm{S/G2/M}} \approx 1.2$), and
950 similar coefficients of variation in G1/S and G2/M sizes ($\rho_{\mathrm{G2/M\ vs.\ G1/S}} \approx 1$). In the
951 simulation, noise terms were $\xi_{\mathrm{C,G1}}, \xi_{\mathrm{C,S/G2/M}}, \xi_{\mathrm{G2/M}} = 0.02; \xi_{\mathrm{G1/S}} = 0.08$.

Table S1.

Average birth size ($\mu_{\mathrm{i,G1}}$) is determined by model parameters. Left: Average birth size for a G2/M two-phase master regulator where growth and regulator production have the same size dependences in both phases $\lambda_g = \lambda_{c,\mathrm{G1}} = \lambda_{c,\mathrm{S/G2/M}}$; Fig. 1A,C), Θ is the threshold level for G2/M, and Θ_{deg} is the fixed level that the regulator is degraded to following G2/M. Middle: Average birth size for a G1/S two-phase master regulator where growth and regulator production have the same size dependencies in both phases ($\lambda_g = \lambda_{c,\mathrm{G1}} = \lambda_{c,\mathrm{S/G2/M}}$). Right: Average birth size for a G1/S inhibitor dilutor that triggers G1/S at a minimum concentration $k_{\mathrm{thres}}$with a growth size dependence that exceeds the regulator production's size dependence as in budding yeast ($\lambda_g - \lambda_{c,\mathrm{S/G2/M}} = 1$). See SI for similar expressions in more general cases.

Average birth size G2/M two-phase master regulator	Average birth size G1/S two-phase master regulator	Average birth size G1/S inhibitor dilutor
$\frac{\Theta - \Theta_{\mathrm{deg}}}{\frac{\kappa_{\mathrm{G1}}}{\gamma}(\sigma^{\tau}-1) + \frac{\kappa_{\mathrm{S/G2/M}}}{\gamma}(\sigma - \sigma^{\tau})}$	$\frac{\Theta - \Theta_{\mathrm{deg}}/\sigma}{\frac{\kappa_{\mathrm{S/G2/M}}}{\gamma}(1-\sigma^{\tau-1}) + \frac{\kappa_{\mathrm{G1}}}{\gamma}(\sigma^{\tau}-1)}$	$\frac{\ln\sigma\,(1-\tau)}{\sigma^{\tau}(\sigma-1)}\,\frac{\kappa_{\mathrm{S/G2/M}}}{\gamma\,k_{\mathrm{thres}}}$

965 **Table S2.**

966 Expressions for the slopes between first-order cell-size fluctuations away from the
967 mean at consecutive G2/Ms and consecutive G1/Ss in the absence of noise (Methods,
968 SI). When the absolute values of these slopes exceed 1, as shown in the colored
969 regions of Figs. 2A and 3A-C, size homeostasis is lost (Methods, Fig. S1). In these
970 figures, cell cycles are controlled by a two-phase master regulator or an inhibitor
971 dilutor of G1/S or G2/M combined with an independently regulated phase, for
972 example, timer, adder, or sizer regulation corresponding to $f_{\mathrm{phase}} = \sigma_{\mathrm{phase}}$, 1, or 0,
973 respectively. Here, we assumed: for two-phase master regulators, production and
974 growth have the same size-dependencies through both phases ($\Delta\lambda = \lambda_g - \lambda_{c,\mathrm{G1}} =$
975 $\lambda_g - \lambda_{c,\mathrm{S/G2/M}}$); growth is exponential, so $\lambda_g = 1$ and $\sigma_{\mathrm{G1}} = \sigma^{\tau}$(Methods, Fig. 1F). For
976 two-phase master regulators, expressions are for no effect of gene copy number on
977 regulator production ($r_{\mathrm{S/G2/M}} = 1$, Fig. 1A), or a strong limiting effect of gene copy
978 number ($r_{\mathrm{S/G2/M}} = 2$). The fully general expressions are in SI.

979

G1/S inhibitor dilutor. Plotted in Fig. 2A with $\Delta\lambda = 1$ (i,iii,v) or $\Delta\lambda = 0$ (ii,iv,vi).

Linear slopes between consecutive G2/M sizes

S/G2/M sizer	*S/G2/M adder*	*S/G2/M timer (exponential growth)*
0	As for G1/S	As for G1/S

Linear slopes between consecutive G1/S sizes

S/G2/M sizer	*S/G2/M adder*	*S/G2/M timer (exponential growth)*
$\frac{1-\frac{(\sigma-1)(1-\Delta\lambda)}{\sigma^{(1-\tau)(1-\Delta\lambda)}-1}}{\sigma}$	$\frac{1+(\sigma^{-(1-\tau)\Delta\lambda}-1)\frac{(\sigma-1)(1-\Delta\lambda)}{\sigma^{(1-\tau)(1-\Delta\lambda)}-1}}{\sigma}$	$\frac{\sigma-\Delta\lambda(\sigma-1)}{\sigma}$

G2/M two-phase master regulator. Plotted in Fig. 3A with $\Delta\lambda = 1$ and $r_{S/G2/M} = 2$.

Linear slopes between consecutive G2/M sizes

	G1 sizer	*G1 adder*	*G1 timer (exponential growth)*
$r_{S/G2/M} = 2$	$\frac{1}{2\sigma^{1-\Delta\lambda}}$	$\frac{1+\sigma^{-\tau\Delta\lambda}}{2\sigma^{1-\Delta\lambda}}$	$\frac{1+\sigma^{\tau(1-\Delta\lambda)}}{2\sigma^{1-\Delta\lambda}}$
$r_{S/G2/M} = 1$	$\frac{1}{\sigma^{1-\Delta\lambda}}$	$\frac{1}{\sigma^{1-\Delta\lambda}}$	$\frac{1}{\sigma^{1-\Delta\lambda}}$

Linear slopes between consecutive G1/S sizes

	G1 sizer	*G1 adder*	*G1 timer (exponential growth)*
$r_{S/G2/M} = 2$	0	As for G2/M	As for G2/M
$r_{S/G2/M} = 1$	0	As for G2/M	As for G2/M

G1/S two-phase master regulator. Plotted in Fig. 3B with $\Delta\lambda = 0$ and $r_{S/G2/M} = 2$; Fig. 3C with $\Delta\lambda = 2$ or $\Delta\lambda = 3$ and $r_{S/G2/M} = 1$.

Linear slopes between consecutive G2/M sizes

	S/G2/M sizer	*S/G2/M adder*	*S/G2/M timer (exponential growth)*
$r_{S/G2/M} = 2$	0	As for G1/S	As for G1/S
$r_{S/G2/M} = 1$	0	As for G1/S	As for G1/S

Linear slopes between consecutive G1/S sizes

	S/G2/M sizer	*S/G2/M adder*	*S/G2/M timer (exponential growth)*
$r_{S/G2/M} = 2$	$\frac{2}{\sigma}$	$\frac{2-\sigma^{\tau\Delta\lambda}(2\sigma^{-\Delta\lambda}-1)}{\sigma}$	$\frac{2-\sigma^{\tau(\Delta\lambda-1)+1}(2\sigma^{-\Delta\lambda}-1)}{\sigma}$
$r_{S/G2/M} = 1$	$\frac{1}{\sigma}$	$\frac{1-\sigma^{\tau\Delta\lambda}(\sigma^{-\Delta\lambda}-1)}{\sigma}$	$\frac{1-\sigma^{\tau(\Delta\lambda-1)+1}(\sigma^{-\Delta\lambda}-1)}{\sigma}$

Methods

Below, the model description of average cellular behaviors included in the Results is extended, then noise, simulations, and analytical derivations are explained.

Models

We study two classes of regulators, with total intracellular level C, that trigger G1/S or G2/M progression and are produced in a potentially size-dependent manner with negligible degradation. Parameters $\lambda_{c,\text{phase}}$ in phases G1 and S/G2/M determine the cell size (S) dependencies of regulator production $\left(\frac{dC}{dt}\right)$ according to

$$\frac{dC}{dt} = \kappa_{\text{phase}}\, S^{\lambda_{c,\text{phase}}}. \quad (9)$$

Master regulators are produced through one or two phases to trigger G1/S or G2/M progression upon reaching a total intracellular threshold level; degradation follows to a fixed level (e.g. zero; analyses show the degraded level has no impact on size homeostasis behaviors, see SI) (Fig. 1A). Inhibitor dilutors are produced throughout one phase and then diluted out in the subsequent phase to trigger G1/S or G2/M at a minimum threshold concentration (Fig. 1A). G2/M and division are assumed to be coincident. Upon division, cells divide symmetrically ($\sigma = 2$) or asymmetrically ($\sigma \neq 2$) in a ratio 1:($\sigma - 1$) and any regulator that persists is inherited in proportion to daughter cell size (Fig. 1B). Hence, at steady state population dynamics, the overall fold-size increase is σ, and division-plane positioning is independent of the preceding birth and G1/S sizes. Analyses and simulations assume steady state population dynamics of one

cell type: following each division, only one daughter cell, corresponding to an average portion size of 1 and not $\sigma - 1$, is retained for analyses or simulations. The cellular growth rate $\left(\frac{dS}{dt}\right)$ depends on cell size according to

$$\frac{dS}{dt} = \gamma S^{\lambda_g} \quad (10)$$

where λ_g determines the growth type (exponential for $\lambda_g = 1$ and linear for $\lambda_g = 0$) and γ sets the average timescale for growth (Fig. 1C).

Master regulators or inhibitor dilutors are often considered in combination with an independently regulated S/G2/M or G1 phase: cell size at the end of the phase ($S_{\mathrm{e,phase}}$) depends on cell size at the beginning of the phase ($S_{\mathrm{i,phase}}$) according to

$$S_{\mathrm{e,phase}} = f_{\mathrm{phase}}\, S_{\mathrm{i,phase}} + (\sigma_{\mathrm{phase}} - f_{\mathrm{phase}})\, \mu_{\mathrm{i,phase}}, \quad (11)$$

where f_{phase} is the mode of control ($f_{\mathrm{phase}} = 0$, 1, or depends on growth behavior for "sizer", "adder", or "timer" control, respectively), $\sigma_{\mathrm{phase}} > 1$ is the average fold-size increase, and $\mu_{\mathrm{i,phase}}$ is the average initial size at steady state (Fig. 1D). The steady state fold-size increase over G1 and S/G2/M are related to the fraction of the cell cycle spent in G1 (τ) by $\sigma_{\mathrm{G1}} \approx \sigma^{\tau}$ and $\sigma_{\mathrm{S/G2/M}} \approx \sigma^{1-\tau}$ because $\sigma_{\mathrm{S/G2/M}} = \sigma/\sigma_{\mathrm{G1}}$. (The approximations are exact for exponential growth where the cell cycle duration is $\ln \sigma/\gamma$, so $\tau = \frac{T}{\ln \sigma}/\gamma$ if T is the average G1 duration and $\sigma_{\mathrm{G1}} = \frac{\mu_{\mathrm{i,S/G2/M}}}{\mu_{\mathrm{i,G1}}} = e^{\gamma T} = e^{\ln \sigma\, \tau} = \sigma^{\tau}$.) A convenient aspect of the model is that the natural choice for free parameters changes as the control type of

the independently regulated phase changes. For example, for an independently regulated phase under timer control, the natural free parameter is the duration of the phase or the fraction of the cell cycle spent in the phase (τ), whereas for critical size or equivalently sizer control, the natural choice is the average cell size at the transition ($\mu_{\mathrm{e,phase}}$). Regardless of the natural choice, at steady state an equation connecting τ and $\mu_{\mathrm{i,phase}}$ or $\mu_{\mathrm{e,phase}}$ (SI) allows us to work in terms of the parameter τ (or σ_{G1}). Then parameter sets that fail to implement cell cycles with two checkpoints on average are straightforward to exclude by enforcing $0 \leq \tau \leq 1$ (Fig. 2A, 3A-C).

More general analyses in SI allow growth and production rates to continually depend on cell size at the beginning of the phase, growth parameters λ_g and γ to differ in G1 vs. S/G2/M, and the threshold mechanisms for cell cycle checkpoint progression to vary.

Simulations and noise

Cells were initialized to the steady-state birth size and regulator level plus noise (SI). Then, cell sizes and regulator levels at G1/S and G2/M were simulated according to specified average cell-cycle control and growth parameters (Eq. 9-11) with 4 noise terms in cell-cycle regulation. We present a specific example; the general case is described in detail in SI. If an inhibitor dilutor triggers G1/S at a threshold concentration (k_{thres}),

1041 then at the end of the G1 dilution phase the regulator level ($C_{\mathrm{G1/S}}$) and cell size ($S_{\mathrm{G1/S}}$)

1042 depend on the regulator level at birth (C_b) as

1043 $$C_{\mathrm{G1/S}} = C_b + k_{\mathrm{thres}}\,\mu_{\mathrm{e,G1}}\,(\sigma - 1)\,Z_{C,\mathrm{G1}}, \qquad S_{\mathrm{G1/S}} = C_{\mathrm{G1/S}}/k_{\mathrm{thres}} + \mu_{\mathrm{e,G1}}\,Z_{\mathrm{G1/S}}$$

1044 where $Z_{C,\mathrm{G1}}$ and $Z_{\mathrm{G1/S}}$ are zero-mean Gaussian noise terms that perturb the level of

1045 inhibitor over the G1 dilution phase and the G1/S threshold concentration, respectively.

1046 The noise terms' coefficients give convenient interpretations for the corresponding

1047 standard deviations (s.d.). For example, $\xi_{\mathrm{G1/S}}$, the s.d. of $Z_{\mathrm{G1/S}}$ (equal to the typical G1/S

1048 error, $e_{\mathrm{G1/S}}$, in Results), approximates the coefficient of variation (CV) of the threshold

1049 concentration (SI). If S/G2/M is independently regulated, at G2/M, the cell size ($S_{\mathrm{G2/M}}$)

1050 and regulator level ($C_{\mathrm{G2/M}}$) are

1051 $$S_{\mathrm{G2/M}} = f_{\mathrm{S/G2/M}}\,S_{\mathrm{G1/S}} + (\sigma_{\mathrm{S/G2/M}} - f_{\mathrm{S/G2/M}})\mu_{i,\mathrm{S/G2/M}} + \mu_{e,\mathrm{S/G2/M}}\,Z_{\mathrm{G2/M}},$$

1052 $$C_{\mathrm{G2/M}} = C_{\mathrm{G1/S}} + \int_{S_{\mathrm{G1/S}}}^{S_{\mathrm{G2/M}} - \mu_{e,\mathrm{S/G2/M}}\,Z_{\mathrm{C,S/G2/M}}} \frac{dC}{dS}\,dS$$

1053 where $Z_{\mathrm{G2/M}}$ is a zero-mean Gaussian noise term that perturbs the G2/M checkpoint,

1054 $\int (dC/dS)\,dS$ is found explicitly from Eq. 9 divided by Eq. 10, and $Z_{C,\mathrm{S/G2/M}}$ is a zero-

1055 mean Gaussian noise term in inhibitor production compared with growth through

1056 S/G2/M. The interpretation of $\xi_{\mathrm{G2/M}}$, the s.d. of $Z_{\mathrm{G2/M}}$, depends on the mode of S/G2/M

1057 control (SI); for example, if the control is sizer ($f_{\mathrm{S/G2/M}} = 0$), $\xi_{\mathrm{G2/M}}$ is the CV in the G2/M

1058 critical cell size. The regulator level and cell size at birth of the retained daughter in the

1059 next generation are

$$C_b' = C_{\mathrm{G2/M}}/\sigma, \qquad S_b' = S_{\mathrm{G2/M}}/\sigma$$

where no noise in division was assumed. Analytical derivations (SI) show that size homeostasis behaviors depend on just two noise-related parameters, $\eta_{\mathrm{G1/S}} = \xi_{\mathrm{G1/S}}/\mathrm{CV}(\text{cell size at G1/S})$ and $\eta_{\mathrm{G2/M}} = \xi_{\mathrm{G2/M}}/\mathrm{CV}(\text{cell size at G1/S})$ (Fig. 1E). In general, the noise terms that cause deviation from the average coupling between inhibitor dynamics and growth, $Z_{C,\mathrm{G1}}$ and $Z_{C,\mathrm{S/G2/M}}$, contribute to cell size at G1/S without affecting $\xi_{\mathrm{G1/S}}$ and $\xi_{\mathrm{G2/M}}$ and thus reduce $\eta_{\mathrm{G1/S}}$ and $\eta_{\mathrm{G2/M}}$.

In simulations, growth is forced to be non-negative over each phase, so $S_{\mathrm{b}} < S_{\mathrm{G1/S}} < S_{\mathrm{G2/M}}$, and regulator levels are forced to be non-negative (SI). This forcing is not included in analytical derivations, yet the derivations are in excellent agreement with simulations, indicating that it has minimal impact on results. Cells were simulated for 30+ generations until steady states were patently reached.

Analysis

Throughout analyses, linear regression slopes between cell-size variables (Eqs. 1-8) were derived as follows: scaled cell-size fluctuations at each transition ($\Delta S_{\mathrm{G1/S}} = S_{\mathrm{G1/S}}/\mu_{e,\mathrm{G1}} - 1$ and $\Delta S_{\mathrm{G2/M}} = S_{\mathrm{G2/M}}/\mu_{e,\mathrm{S/G2/M}} - 1$) were expressed in terms of scaled size fluctuations at earlier transitions, then only linear terms from a Taylor expansion and noise terms were retained for analyses, because cell size fluctuations are small (in most

measurements, the coefficient of variation in cell size is ~0.13 (Cadart, 2018; Cadart et al., 2018; Taheri-Araghi et al., 2015; Willis et al., 2016)) and noise terms are comparable in magnitude to cell size fluctuations (Amir, 2014). Indeed, analytically derived linear regression slopes are in excellent agreement with simulations with realistic noise levels, indicating that the linear approximation is appropriate (Fig. 2-4).

We present two examples; the general case is detailed in SI. For a one-phase master regulator produced from a fixed level at G1/S through S/G2/M to trigger G2/M when it is degraded, the linearized relationship between $\Delta S_{\mathrm{G1/S}}$ and $\Delta S_{\mathrm{G2/M}}$ is found by solving Eqs. 9 and 10 followed by a Taylor expansion,

$$\Delta S_{\mathrm{G2/M}} = \sigma_{\mathrm{S/G2/M}}^{\Delta\lambda-1}\ \Delta S_{\mathrm{G1/S}} + Z_{\mathrm{G2/M}} + Z_{C,\mathrm{S/G2/M}} + \text{higher order terms} \quad (12)$$

where $\Delta\lambda = \lambda_g - \lambda_{c,\mathrm{S/G2/M}}$. By definition, the linear regression slope between G1/S and G2/M sizes ($l_{\mathrm{S/G2/M}}$) is

$$l_{\mathrm{S/G2/M}} = \frac{\mathbf{E}[(S_{\mathrm{G2/M}} - \mu_{e,\mathrm{S/G2/M}})(S_{\mathrm{G1/S}} - \mu_{e,\mathrm{G1}})]}{\mathbf{E}[(S_{\mathrm{G1/S}} - \mu_{e,\mathrm{G1}})^2]} = \frac{\sigma_{\mathrm{S/G2/M}}\,\mathbf{E}[\Delta S_{\mathrm{G2/M}}\Delta S_{\mathrm{G1/S}}]}{\mathbf{E}[(\Delta S_{\mathrm{G1/S}})^2]} \quad (13)$$

where $\mathbf{E}[\cdot]$ denotes the average (SI). So, the slope $l_{\mathrm{S/G2/M}}$ is computed by multiplying Eq. 12 by $\sigma_{\mathrm{S/G2/M}}\Delta S_{\mathrm{G1/S}}$, taking averages of each side of the equation, and dividing by $\mathbf{E}[(\Delta S_{\mathrm{G1/S}})^2]$. Since G1/S size fluctuations ($\Delta S_{\mathrm{G1/S}}$) are independent of noise in the subsequent G2/M threshold ($Z_{\mathrm{G2/M}}$) and regulator dynamics compared with growth

over S/G2/M ($Z_{C,\mathrm{S/G2/M}}$), upon taking averages, the noise terms disappear. Thus, the linear regression slope between G1/S and G2/M sizes is

$$l_{\mathrm{S/G2/M}} = \sigma^{\Delta\lambda}_{\mathrm{S/G2/M}}.$$

From the definition of independently regulated phases (Eq. 11) with noise, after rearrangement, we have

$$\Delta S_{\mathrm{G2/M}} = \frac{f_{\mathrm{S/G2/M}}}{\sigma_{\mathrm{S/G2/M}}}\Delta S_{\mathrm{G1/S}} + Z_{\mathrm{G2/M}}.$$

Again, the linear regression slope between G1/S and G2/M sizes is computed according to Eq. 13, to give

$$l_{\mathrm{S/G2/M}} = f_{\mathrm{S/G2/M}}.$$

Eqs. 1-8 were derived similarly but often the dependence of size fluctuations on noise terms in preceding phases causes noise to affect size homeostasis behaviors (SI). Importantly, throughout the analytical derivations, no assumptions were made about the distributions of $Z_{\mathrm{G1/S}}$, $Z_{\mathrm{C,G1}}$, $Z_{\mathrm{G2/M}}$, and $Z_{\mathrm{C,S/G2/M}}$ beyond the values of their standard deviations, indicating that, for small fluctuations in cell size, further properties of the distributions (e.g. skewness) have no effect on size homeostasis behaviors.

Conditions for the loss of size homeostasis

Derivations of the type above led to first-order expressions connecting size fluctuations at G1/S and G2/M in consecutive cell cycles

$$\Delta S'_{\mathrm{G1/S}} = \alpha \Delta S_{\mathrm{G1/S}} + \text{noise terms}$$

$$\Delta S'_{\mathrm{G2/M}} = \beta \Delta S_{\mathrm{G2/M}} + \text{noise terms}$$

where ' denotes the subsequent cell cycle, and α and β are functions of parameters (SI). These equations establish whether fluctuations from the average cell size diverge, so that size homeostasis is lost, even in the absence of noise according to whether $|\alpha| \geq 1$ or $|\beta| \geq 1$ for G1/S or G2/M, respectively (Fig. S1). The colored regions of Fig. 2A and 3A-C show where $|\alpha| \geq 1$ or $|\beta| \geq 1$ for the parameters specified in each plot. Simulations of single-cell trajectories with $|\alpha| \approx 1$ and $|\beta| \approx 1$, i.e. close to the boundary of size homeostasis, show that size homeostasis is compromised (Fig. 2B, 3D, S2), thus supporting our analyses.

General expressions for size-homeostasis statistics

The full model features up to 22 parameters (SI). This space is too large to explore computationally. Analytical derivations effectively shrunk the parameter space, because only certain parameter combinations affect size homeostasis statistics. Table S2 and Eqs. 1—8 exemplify specific cases where size homeostasis statistics depend on a parameter set that is effectively strongly reduced, with fully general expressions derived in SI.

Regardless of the nature of cell cycle control, the linear regression slope between scaled fluctuations in the duration of the phase and scaled size fluctuations at the beginning of the phase is

$$\frac{1-\lambda_g}{\sigma_{\text{phase}}-\sigma_{\text{phase}}^{\lambda_g}}\left(l_{\text{phase}}-\sigma_{\text{phase}}^{\lambda_g}\right)$$

where l_{phase} is the linear regression slope between cell size at the beginning vs. cell size at the end of the phase (SI). This slope must be zero for independently regulated timer phases, thus, $l_{\text{phase}} = f_{\text{phase}} = \sigma_{\text{phase}}^{\lambda_g}$.

References

Amir, A. (2014). Cell size regulation in bacteria. Phys Rev Lett *112*, 208102.

Barber, F., Ho, P.Y., Murray, A.W., and Amir, A. (2017). Details matter: noise and model structure set the relationship between cell size and cell cycle timing. Front Cell Dev Biol *5*.

Cadart, C. (2018). Personal communication.

Cadart, C., Monnier, S., Grilli, J., Attia, R., Terriac, E., Baum, B., Cosentino-Lagomarsino, M., and Piel, M. (2018). Size control in mammalian cells involves modulation of both growth rate and cell cycle duration. Nat Commun *9*, 3275.

Campos, M., Surovtsev, I.V., Kato, S., Paintdakhi, A., Beltran, B., Ebmeier, S.E., and Jacobs-Wagner, C. (2014). A constant size extension drives bacterial cell size homeostasis. Cell *159*, 1433-1446.

Chandler-Brown, D., Schmoller, K.M., Winetraub, Y., and Skotheim, J.M. (2017). The adder phenomenon emerges from independent control of pre- and post-start phases of the budding yeast cell cycle. Curr Biol *27*, 2774—2783.

Coudreuse, D., and Nurse, P. (2010). Driving the cell cycle with a minimal CDK control network. Nature *468*, 1074-1079.

Cross, F.R. (1988). DAF1, a mutant gene affecting size control, pheromone arrest, and cell cycle kinetics of *Saccharomyces cerevisiae*. Mol Cell Biol *8*, 4675—4684.

1162 Dewitte, W., Riou-Khamlichi, C., Scofield, S., Healy, J.M., Jacqmard, A., Kilby, N.J., and
1163 Murray, J.A. (2003). Altered cell cycle distribution, hyperplasia, and inhibited
1164 differentiation in Arabidopsis caused by the D-type cyclin CYCD3. Plant Cell *15*, 79-92.
1165 Di Talia, S., Skotheim, J.M., Bean, J.M., Siggia, E.D., and Cross, F.R. (2007). The effects of
1166 molecular noise and size control on variability in the budding yeast cell cycle. Nature
1167 *448*, 947-951.
1168 Eun, Y.-J., Ho, P.-Y., Kim, M., LaRussa, S., Robert, L., Renner, L.D., Schmid, A., Garner,
1169 E., and Amir, A. (2018). Archaeal cells share common size control with bacteria despite
1170 noisier growth and division. Nat Microbiol *3*, 148—154.
1171 Facchetti, G., Knapp, B., Flor-Parra, I., Chang, F., and Howard, M. (2019).
1172 Reprogramming cdr2-dependent geometry-based cell size control in fission yeast. Curr
1173 Biol *29*, 350–358.
1174 Fantes, P.A. (1977). Control of cell size and cycle time in *Schizosaccharomyces pombe*. J
1175 Cell Sci *24*, 51-67.
1176 Ginzberg, M.B., Chang, N., D'Souza, H., Patel, N., Kafri, R., and Kirschner, M.W. (2018).
1177 Cell size sensing in animal cells coordinates anabolic growth rates and cell cycle
1178 progression to maintain cell size uniformity. ELife *11*, e26957.
1179 Harashima, H., Dissmeyer, N., and Schnittger, A. (2013). Cell cycle control across the
1180 eukaryotic kingdom. Trends in Cell Biology *23*, 345-356.

1181 Harashima, H., and Sugimoto, K. (2016). Integration of developmental and
1182 environmental signals into cell proliferation and differentiation through
1183 RETINOBLASTOMA-RELATED 1. Curr Opin Plant Biol *29*, 95–103.
1184 Heldt, F.S., Lunstone, R., Tyson, J.J., and Novák, B. (2018). Dilution and titration of cell-
1185 cycle regulators may control cell size in budding yeast. PLOS Comput Biol *14*, e1006548.
1186 Hilfinger, A., and Paulsson, J. (2011). Separating intrinsic from extrinsic fluctuations in
1187 dynamic biological systems. Proc Natl Acad Sci USA *108*, 12167–12172.
1188 Ho, P.-Y., and Amir, A. (2015). Simultaneous regulation of cell size and chromosome
1189 replication in bacteria. Front Microbiol *6*, 662.
1190 Hochegger, H., Takeda, S., and Hunt, T. (2008). Cyclin-dependent kinases and cell-cycle
1191 transitions: does one fit all? Nat Rev Mol Cell Biol *9*, 910–916.
1192 Jones, A.R., Forero-Vargas, M., Withers, S.P., Smith, R.S., Traas, J., Dewitte, W., and
1193 Murray, J.A.H. (2017). Cell-size dependent progression of the cell cycle creates
1194 homeostasis and flexibility of plant cell size. Nat Commun *8*, 15060.
1195 Keifenheim, D., Sun, X., D'Souza, E., Ohira, M.J., Magner, M., Mayhew, M.B.,
1196 Marguerat, S., and Rhind, N. (2017). Size-dependent expression of the mitotic activator
1197 Cdc25 suggests a mechanism of size control in fission yeast. Curr Biol *27*, 1491—1497.
1198 Lin, J., and Amir, A. (2018). Homeostasis of protein and mRNA concentrations in
1199 growing cells. Nat Commun *9*, 4496.

Logsdon, M.M., Ho, P.Y., Papavinasasundaram, K., Richardson, K., Cokol, M., Sassetti, C.M., Amir, A., and Aldridge, B.B. (2017). A parallel adder coordinates mycobacterial cell-cycle progression and cell-size homeostasis in the context of asymmetric growth and organization. Curr Biol *27*, 3367—3374.

Micali, G., Grilli, J., Marchi, J., Osella, M., and Cosentino Lagomarsino, M. (2018a). Dissecting the control mechanisms for DNA replication and cell division in *E. coli*. Cell Rep *25*, 761.

Micali, G., Grilli, J., Osella, M., and Lagomarsino, M.C. (2018b). Concurrent processes set E. coli cell division. Sci Adv *4*, eaau3324.

Newman, J.R., Ghaemmaghami, S., Ihmels, J., Breslow, D.K., Noble, M., DeRisi, J.L., and Weissman, J.S. (2006). Single-cell proteomic analysis of *S. cerevisiae* reveals the architecture of biological noise. Nature *441*, 840—846.

Nordholt, N., van Heerden, J.H., and Bruggeman, F.J. (2019). Growth-rate and protein-synthesis dynamics of single Bacillus subtilis cells along their cell-cycle. bioRxiv.

Osella, M., Nugent, E., and Cosentino Lagomarsino, M. (2014). Concerted control of *Escherichia coli* cell division. Proc Natl Acad Sci USA *111*, 3431-3435.

Padovan-Merhard, O., Nair, G.P., Biaesch, A.G., Mayer, A., Scarfone, S., Foley, S.W., Wu, A.R., Churchman, L.S., Singh, A., and Raj, A. (2015). Single mammalian cells compensate for differences in cellular volume and DNA copy number through independent global transcriptional mechanisms. Mol Cell *58*, 339—352.

1220 Pan, K.Z., Saunders, T.E., Flor-Parra, I., Howard, M., and Chang, F. (2014). Cortical
1221 regulation of cell size by a sizer cdr2p. eLife *3*.
1222 Patterson, J.O., Rees, P., and Nurse, P. (2019). Noisy cell-size correlated expression of
1223 Cyclin B drives probabilistic cell-size homeostasis in fission yeast. Curr Biol *29*, 1379–
1224 1386.
1225 Schmoller, K.M., and Skotheim, J.M. (2015). The biosynthetic basis of cell size control.
1226 Trends Cell Biol *25*, 793-802.
1227 Schmoller, K.M., Turner, J.J., Koivomagi, M., and Skotheim, J.M. (2015). Dilution of the
1228 cell cycle inhibitor Whi5 controls budding-yeast cell size. Nature *526*, 268-272.
1229 Scofield, S., Jones, A., and Murray, J.A.H. (2014). The plant cell cycle in context. J Exp
1230 Bot *65*, 2557–2562.
1231 Sekar, K., Rusconi, R., Sauls, J.T., Fuhrer, T., Noor, E., Nguyen, J., Fernandez, V.I.,
1232 Buffing, M.F., Berney, M., Jun, S., *et al.* (2018). Synthesis and degradation of FtsZ
1233 quantitatively predict the first cell division in starved bacteria. Mol Syst Biol *14*, e8623.
1234 Shi, H., Colavin, A., Bigos, M., Tropini, C., Monds, R.D., and Huang, K.C. (2017). Deep
1235 phenotypic mapping of bacterial cytoskeletal mutants reveals physiological robustness
1236 to cell size. Curr Biol *27*, 3419—3429.
1237 Si, F., Treut, G.L., Sauls, J.T., Vadia, S., Levin, P.A., and Jun, S. (2019). Mechanistic origin
1238 of cell-size control and homeostasis in bacteria. Curr Biol *29*, 1–11.

1239 Soifer, I., Robert, L., and Amir, A. (2016). Single-cell analysis of growth in budding yeast
1240 and bacteria reveals a common size regulation strategy. Curr Biol *26*, 356-361.
1241 Swaffer, M.P., Jones, A.W., Flynn, H.R., Snijders, A.P., and Nurse, P. (2016). CDK
1242 substrate phosporylation and ordering in the cell cycle. Cell *167*, 1750—1761.
1243 Taheri-Araghi, S., Bradde, S., Sauls, J.T., Hill, N.S., Levin, P.A., Paulsson, J., Vergassola,
1244 M., and Jun, S. (2015). Cell-size control and homeostasis in bacteria. Curr Biol *25*, 385-
1245 391.
1246 Turner, J.J., Ewald, J.C., and Skotheim, J.M. (2012). Cell size control in yeast. Curr Biol
1247 *22*, 350-359.
1248 Varsano, G., Wang, Y., and Wu, M. (2017). Probing Mammalian Cell Size Homeostasis
1249 by Channel-Assisted Cell Reshaping. Cell Rep *20*, 397—410.
1250 Wallden, M., Fange, D., Lundius, E.G., Baltekin, Ö., and Elf, J. (2016). The
1251 synchronization of replication and division cycles in individual *E. coli* cells. Cell *166*,
1252 729-739.
1253 Wang, P., Robert, L., Pelletier, J., Dang, W.L., Taddei, F., Wright, A., and Jun, S. (2010).
1254 Robust growth of *Escherichia coli*. Curr Biol *20*, 1099-1103.
1255 Willis, L., and Huang, K. (2017). Sizing-up the bacterial cell cycle. Nat Rev Microbiol *15*,
1256 606–620.

1257 Willis, L., Refahi, Y., Wightman, R., Landrein, B., Teles, J., Huang, K.C., Meyerowitz,

1258 E.M., and Jönsson, H. (2016). Cell size and growth regulation in the A*rabidopsis thaliana*

1259 apical stem cell niche. Proc Nat Acad Sci *113*, E8238—8246.

1260